



Enhancing the H₂O Megamaser Detection Rate Using Optical and Mid-infrared Photometry

C. Y. Kuo¹ , A. Constantin² , J. A. Braatz³, H. H. Chung¹, C. A. Witherspoon², D. Pesce⁴ , C. M. V. Impellizzeri^{3,5},
F. Gao⁶, Lei Hao⁷ , J.-H. Woo⁸, and Ingyin Zaw⁹

¹ Physics Department, National Sun Yat-Sen University, No. 70, Lien-Hai Rd, Kaosiung City 80424, Taiwan, R.O.C

² Department of Physics and Astronomy, James Madison University, Harrisonburg, VA 22807, USA

³ National Radio Astronomy Observatory, 520 Edgemont Road, Charlottesville, VA 22903, USA

⁴ Department of Astronomy, University of Virginia, Charlottesville, VA 22904, USA

⁵ Joint Alma Office, Alonso de Cordova 3107, Vitacura, Santiago, Chile

⁶ Max Planck Institute for Extraterrestrial Physics, Giessenbach str., D-85748, Garching, Germany

⁷ Shanghai Astronomical Observatory, Chinese Academy of Sciences, Shanghai 200030, People's Republic of China

⁸ Astronomy Program, Department of Physics and Astronomy, Seoul National University, Seoul 151-742, Republic of Korea

⁹ New York University Abu Dhabi, Abu Dhabi, UAE

Received 2017 December 12; revised 2018 May 11; accepted 2018 May 12; published 2018 June 25

Abstract

Water megamasers from circumnuclear disks in galaxy centers provide the most accurate measurements of supermassive black hole masses and uniquely probe the subparsec accretion processes. At the same time, these systems offer independent crucial constraints of the Hubble constant in the nearby universe, and thus, the arguably best single constraint on the nature of dark energy. The chances of finding these golden standards are, however, abysmally low, at $\lesssim 3\%$ overall for any level of water maser emission detected at 22 GHz and $\lesssim 1\%$ for those exhibiting disk-like configuration. We provide here a thorough summary of the current state of detection of water megamaser disks along with a novel investigation of the likelihood of increasing their detection rates based on a multivariate parameter analysis of the optical and mid-infrared (mid-IR) photometric properties of the largest database of galaxies surveyed for 22 GHz emission. We find that galaxies with water megamaser emission tend to be associated with strong emission in all *Wide-field Infrared Survey Explorer* mid-IR wavelengths, with the strongest enhancement in the W4 band, at 22 μm , as well as with previously proposed and newly found indicators of active galactic nucleus strength in the mid-IR, such as red W1 – W2 and W1 – W4 colors, and the integrated mid-IR luminosity of the host galaxy. These trends offer a potential boost of the megamaser detection rates to 6%–15%, or a factor of 2–8 relative to the current rates, depending on the chosen sample selection criteria, while fostering real chances for discovering $\gtrsim 20$ new megamaser disks.

Key words: galaxies: active – galaxies: nuclei – infrared: galaxies – masers – surveys

1. Introduction

Astrophysical water masers are natural microwave amplifiers by stimulated emission of radiation. When detected in galaxy centers and extremely luminous, i.e., millions of times more luminous (brightness temperatures to 10^{16} K; isotropic luminosities $L_{\text{H}_2\text{O}} \gtrsim 10 L_\odot$) than those associated with typical star-forming regions in the spiral arms of our own Milky Way, they are termed “megamasers.” For a fraction ($\sim 30\%$) of them, disk-maser candidates are identified via the high-velocity features (redshifted and blueshifted features) that their 22 GHz spectra show in addition to the systemic velocity components (e.g., Kondratko et al. 2006; Kuo et al. 2011). Water megamasers in a disk-like configuration are a treasure trove, for they advance our understanding of two extremely important issues: (i) the current cosmological model and the nature of dark energy (DE), and (ii) galaxy formation and evolution processes.

Vital constraints on the current cosmological model need an extremely accurate Hubble constant H_0 value. The exquisite *WMAP* cosmic microwave background radiation and *Planck* data from redshifts $z \approx 1100$, when DE was negligible, are consistent with a wide range of values of H_0 if one does not assume that the universe is flat, i.e., the current “concordance” model (Spergel et al. 2007). There is, however, tension between the predicted values of H_0 from *Planck* and observed values based on standard candles (e.g., Riess et al. 2016) or

strong lensing (Bonvin et al. 2017). Thus, independent methods of measuring H_0 are needed in order to minimize systematic uncertainties and ultimately to provide strong constraints of the geometry and the fraction (Ω_m) of the critical density contributed by matter. A 3% or better accuracy in measuring H_0 would arguably provide the best single constraint on the nature of DE where its effect is greatest (Hu 2005; Olling 2007). One way of reaching this level of accuracy is, for example, to measure $\sim 10\%$ distances to each of ≈ 10 galaxies at distances of ~ 50 – 200 Mpc (e.g., Greenhill 2004). To accomplish this goal, we must, however, first identify these precious maser disks, and this requires a substantial increase in their current detection efficiency, which is one of the main objectives of this study.

With regard to the galaxy evolution processes, megamaser disks provide essential means of constraining the supermassive black hole (SMBH) occupation fraction, along with the universality (i.e., the overall shape and scatter) of the empirically found black hole–host galaxy scaling relations,¹⁰ especially on the lower end of the distribution ($M_{\text{BH}} \leq 10^7 M_\odot$), where very few accurate estimates are available (e.g., Greene et al. 2010, 2016). Due to their well-measured Keplerian rotation, the megamaser

¹⁰ The $M_{\text{BH}}-\sigma^*$ relation, e.g., Gebhardt et al. (2000), Ferrarese & Merritt (2000), Tremaine (2002), Gültekin et al. (2009), Graham et al. (2011); and the $M_{\text{BH}}-L_{\text{bulge}}$ relation, e.g., Marconi & Hunt (2003).

disks are an optimal dynamical tracer of the central mass lurking in galaxy centers. Accurate maser-based BH mass measurements via Very Long Baseline Interferometry (VLBI) observations do not suffer from biases from nonvirial gas support (e.g., due to turbulence; Barth et al. 2001). Moreover, unlike stellar dynamical methods, the VLBI measurements are not sensitive to assumptions about galaxy anisotropy and radial variation in dark matter fraction (which are not well constrained observationally; Gebhardt & Thomas 2009; van den Bosch & de Zeeuw 2010).

Unfortunately, from the $\gtrsim 4000$ galaxy nuclei surveyed so far for water maser emission in 22 GHz, only ~ 160 have been detected, with $\sim 30\%$ of them possibly originating in disks. The latest data on water maser surveys are curated and made publicly available by the Megamaser Cosmology Project (MCP).¹¹ Only ~ 40 of all these maser galaxies show “triple” spectra, i.e., displaying systemic and high-velocity emission in three line complexes, and only ~ 10 are possibly good candidates for distance measurements, depending on the collecting area available for VLBI; only < 9 of these objects lie at distances $D > 50$ Mpc, where their peculiar motions are a small fraction of their total motions, thus allowing estimates of H_0 directly from maser distances and recessional velocities (Kuo et al. 2011, 2013, 2015; Reid et al. 2013; Gao et al. 2016).

Good megamaser disk candidates are therefore extremely few. The need to have a disk structure strong enough to enable VLBI imaging throughout the velocity ranges of each complex, combined with the requirement for not only the presence of very dense molecular gas but also a suitable viewpoint, with the nuclear disk seen almost edge-on, causes the probability of detecting the “right” megamaser to drop significantly. Detailed studies of these precious few maser disks clearly identify a parsec-scale Keplerian rotation profile, and accelerations measured with the Green Bank Telescope (GBT) and the VLBI mappings, together with refinements in the acceleration modeling and a 3D disk fitting (Humphreys et al. 2008, 2013), already offer a $\sim 10\%$ uncertainty in H_0 (e.g., Braatz et al. 2010; Kuo et al. 2011, Reid et al. 2013). To increase the accuracy to $< 10\%$, the current suite of telescopes needs an improvement in sensitivity by a factor of ~ 2 , which will not be possible for at least another few decades.

1.1. Megamasers and Their Hosts: Optical Studies and Their Limitations

Initial surveys for maser activity in extragalactic sources have been closely driven by the idea that the maser emission must be associated with intense star formation and thus targeted objects with large infrared emission or unusually active, radio loud, or morphologically peculiar galaxies. Maser emission was detected, albeit extremely rarely, at the rate of < 1 in ~ 40 targets (Batchelor et al. 1982; Henkel et al. 1984, 1986; Whiteoak & Gardner 1986; Hagiwara et al. 2002, 2003; Nakai et al. 2002). These searches revealed that the very few powerful megamasers found were hosted by galaxies with actively accreting SMBHs in their centers (i.e., active galactic nuclei, AGNs), where the maser emission originates within about 1 pc (3 lt-yr) or less of the nucleus (e.g., Claussen & Lo 1986; Haschick et al. 1994); these findings led more recent searches for H_2O megamasers to focus on AGNs. Improved sensitivity and newer spectrometers resulted in new detections in AGNs;

however, the success rate remained a mere $\sim 3\%–5\%$ (Braatz et al. 1996, 1997, 2004, 2010; Greenhill et al. 2003; Kondratko et al. 2006; Braatz & Gugliucci 2008).

To date, almost all megamaser disk sources have been found in galaxies that only show narrow emission-line activity in their centers (i.e., type 2 AGNs, which include both Seyferts and some Low Ionization Nuclear Emission Regions, or LINERs); with extremely few exceptions, AGNs with broad emission (type 1) do not appear to host masers. The standard interpretation for the difference between broad- and narrow-line emission AGNs is known as the “unification scenario” (Antonucci & Miller 1985), where a dusty torus surrounds the nucleus and obscures the central engine (BH, accretion disk, and the broad-line emission region) for large inclination angles. Because the presence of water molecules requires a dusty environment, it has thus been inferred that masers might trace molecular material associated with this torus or with an accretion disk that feeds the nucleus. Consequently, the maser emission is expected to also be heavily geometry dependent in the same manner as type 1/type 2 AGN classes, i.e., to occur for certain, very restricted, viewing angles, perhaps where the line of sight is along the plane of the molecular disk or torus. This scenario appears to be confirmed in great detail by VLBI observations of the megamaser in NGC 4258 (Greenhill et al. 1995; Miyoshi et al. 1995; Lo 2005). Thus, there are good reasons for searching for megamasers in type 2 AGNs.

Nevertheless, there is not enough reason to restrict the megamaser search to narrow-line AGNs—or to previously identified AGNs, for that matter. While there is increasing evidence that the maser disk emission is very likely to originate from a geometrically thin disk made of a large number of molecular clouds that connect the inner edge of the torus and the outer part of the accretion disk (e.g., Masini et al. 2016), there are only very few special cases¹² for which information constraining the inclinations of individual AGN accretion disks relative to that of the surrounding torus is available. The fact that, e.g., the H_2O megamaser (albeit not a disk) emitting quasar MG J0414+0534 shows broad emission (Impellizzeri et al. 2008) proves that broad-line AGNs could also host megamasers. Whether or not all powerful masers host a disk still remains to be identified; however, the presence of a torus does not seem to play as crucial a role in amplifying the radiation as originally thought.

The detailed characterization of the optical properties of the H_2O maser host galaxies (Zhu et al. 2011 and Constantin 2012) provides promising ways of identifying more concrete criteria for searching for H_2O megamasers. These studies also show somewhat surprising trends in their host properties: megamasers are preferentially found in galaxies with strong intrinsic [O III] $\lambda 5007$ emission and high levels of obscuration as measured by Balmer decrements, while they tend to favor a possible “goldilocks” range in other properties, e.g.: (1) a narrow range of $L_{[O III]}/\sigma^{*4}$ values, or Eddington ratios, which suggests a narrow range in their BH accretion rates (concentrated at $L/L_{\text{Edd}} \sim 10^{-2}$), and (2) a narrow distribution of [S II] $\lambda 6716/\lambda 6731$ line ratios, which implies narrow ranges in the electron densities in the line-emitting gas. Maser searches tailored on these findings can potentially result in an approximately fourfold increase of the maser detection rate (to $\gtrsim 11\%$, from the current $< 3\%$). Unfortunately, there are

¹¹ <https://safe.nrao.edu/wiki/bin/view/Main/MegamaserCosmologyProject>

¹² Hutchings et al. (1998), Crenshaw et al. (2000, 2010), Ruiz et al. (2001), Das et al. (2006), Fischer et al. (2010).

very few spectroscopically confirmed galaxies inside this set of properties (e.g., in the Sloan Digital Sky Survey; SDSS), and this sample has been somewhat exhausted (see, e.g., the discussion in van den Bosch et al. 2016).

Interestingly, it is also possible that the high maser detection rate among Seyferts ($\sim 8\%$) may not be due entirely to a genuine connection to this type of activity, as it is enhanced by biases associated with the recent maser surveys that targeted almost exclusively type 2 Seyferts (Constantin 2012). Also, the overall maser detection rate is nonzero for non-AGN types; in fact, there is an equal probability of finding masers among Transition Objects (which straddle the borders between starburst galaxies and AGNs in emission-line diagnostic diagrams; e.g., Baldwin et al. 1981; Veilleux & Osterbrock 1987; Kewley et al. 2006) as in LINERs ($\sim 1.6\%$), and it is twice as likely to find them in star-forming galaxies (or H IIs; $\sim 3\%$). For some of these, the maser luminosity is only a smidgen below the $10 L_{\odot}$ limit that generally (albeit arbitrarily) defines the megamaser activity, and we now have increasing evidence and reasonable physical explanations for variability in megamaser disks (e.g., Pesce et al. 2015), suggesting that these systems might turn into the next disk detection with new observations.

Moreover, if indeed there is an evolutionary sequence in which galaxies transform from star forming via AGN to quiescent as suggested by several studies (Schawinski et al. 2007, 2010; Constantin et al. 2008, 2009, 2015; Cen 2012), accretion onto the central BH should happen as early as the star formation (or H II) phase and should be active in Transition Objects. Thus, if maser activity is related to accretion, we should look for maser disks in H IIs and Transition Objects as well, especially if the evolutionary sequence resembles H II \rightarrow Transition Object \rightarrow Seyfert \rightarrow LINER. The accreting BH could either be obscured by large amounts of dust in the surrounding star-forming regions, or simply optically hidden in a mix of other ionization sources (shocks, turbulence, etc.), or host galaxy light. Hence, restricting our searches to Seyferts and LINERs could overlook a good portion, or even the lion's share, of megamasers. This idea is supported by the detection of a megamaser ostensibly in a star-forming (H II) galaxy (NGC 2989; Braatz & Gugliucci 2008), and another one in a galaxy that was not previously identified as an AGN (UGC 3789; Braatz et al. 2010).

1.2. Megamasers and Their Hosts: X-Ray and Radio Studies

Water maser hosts have been scrutinized outside optical wavelengths as well, most prominently in X-ray and radio wavelengths. Such studies offer some important clues to the connection between water maser emission and AGN activity; however, they have addressed almost exclusively the maser emission in type 2 Seyferts and for rather small number statistics.

To date, 56 masing galaxies that have been investigated in 2–10 keV (Zhang et al. 2006, 2010; Greenhill et al. 2008, Castangia et al. 2013; Masini et al. 2016) suggest that the masers are found in sources with large absorbing column densities ($N_{\text{H}} > 10^{23} \text{ cm}^{-2}$) at a significance level of 95%. Intriguingly, however, these studies also find that the available (small) subsamples of nuclear low-luminosity (or kilo-) masers ($L_{\text{H}_2\text{O}} < 10 L_{\odot}$) and disk megamasers show average neutral hydrogen column densities that are indistinguishable from those of the entire megamaser sample and from, e.g., samples of narrow-line Seyfert galaxies that were not selected with respect to maser

emission. Potentially, a clumpy cloud structure in the circumnuclear environment, diverging positions between maser and nuclear sources, and/or an occasional amplification of a background radio continuum source sufficiently decouples X-ray-measured column densities and H_2O maser properties to mask a clear correlation. It is also possible that any observed association between H_2O megamaser emission and high X-ray column densities may be subject to selection effects: there are only a handful of galaxies that have both quality maser maps and hard X-ray coverage available, which allow for accurate estimates of $N_{\text{H}} > 10^{24} \text{ cm}^{-2}$ values, and thus for which it is possible to establish meaningful connections between the properties of the masing disk and those of the obscuring torus. They are also among the nearest of the sample of galaxies searched for maser activity, and they do not comprise a complete sample by any means (e.g., Masini et al. 2016).

Radio investigations of maser host galaxies appear to bring additional support to the importance of the AGN activity in the centers of these galaxies. Comparisons of the radio emission in maser hosts and a control sample of Seyfert 2s show that the maser galaxies exhibit multiband radio luminosities that are higher than those of non-masers by a factor of a few; however, there seems to be no statistical difference in their spectral indices (Zhang et al. 2012; Liu et al. 2017). If nuclear radio continuum luminosity is an indicator of AGN power (Diamond-Stanic et al. 2009), these findings suggest that AGN activity and its strength may play an important role in exciting strong H_2O megamaser emissions.

Nevertheless, these studies do not answer the question of whether water megamasers are always produced in association with an AGN or whether the maser emission is associated with unrecognized AGN activity (i.e., low-luminosity or obscured AGNs). Also, the possibility of the megamaser activity being connected to other nuclear properties of their host galaxies remains relatively unexplored.

1.3. The Power of the Wide-field Infrared Survey Explorer (WISE) in Identifying New Megamasers

Assuming that all megamaser disks are associated with SMBH accretion, we would need to understand why some types of AGNs are more prone to hosting maser disks than others, even within those classified as type 2. Because hot dust surrounding AGNs produces a strong mid-infrared (mid-IR) continuum and an infrared spectral energy distribution (SED) that is clearly distinguishable from normal star-forming galaxies for both obscured and unobscured AGNs in galaxies where the emission from the AGN dominates over the host galaxy emission, mid-IR observations offer reliable diagnostics for discovering elusive AGNs (e.g., Lacy et al. 2004; Stern et al. 2005, 2012; Alonso-Herrero et al. 2006; Donley et al. 2007; Assef et al. 2013). Thus, by employing a systematic study of the mid-IR properties of known maser and non-maser galaxies, we are bound to constrain the means by which the obscuring torus and the masing disk are related. By investigating how the dust properties compare among different maser strengths and morphologies, we might be able to find out whether a dusty torus is necessary for strong maser disk emission. Would they reflect similar or different temperature ranges, and thus different mid-IR SEDs and colors? Would any similarities or differences in their mid-IR characteristics help us build more efficient maser disk surveys?

The all-sky survey carried out by *WISE* (Wright et al. 2010) has opened up a new window in the search for optically hidden AGNs in a large number of galaxies. In particular, for low-redshift galaxies, the $W1(3.4\ \mu\text{m}) - W2(4.6\ \mu\text{m})$ color in objects where emission is dominated by AGNs is considerably redder ($\gtrsim 0.8$) than that of inactive galaxies (see Figure 1 in Stern et al. 2012; Assef et al. 2013). While this criterion alone would likely identify heavily obscured Compton-thick sources that are expected to be good places to search for H_2O megamasers (Zhang et al. 2006; Greenhill et al. 2008; Castangia et al. 2013), it loses its reliability at fainter fluxes (Assef et al. 2013). Lower-luminosity AGNs (e.g., with Eddington ratios $\lesssim 10^{-2}$), where strong disk-maser systems often reside (Constantin 2012), can be easily missed by this simple selection criterion (Gao et al. 2017). We are exploring here for the first time a wide variety of the *WISE* mid-IR photometric properties that could be used as megamaser diagnostics.

Adding information from optical bands has increased the success of mid-IR photometric searches for elusive low-luminosity AGNs (e.g., Fiore et al. 2008; Georgantopoulos et al. 2008; Rovilos et al. 2011), and we also probe here these effects on increasing the megamaser detection rates as well. In particular, an enhanced $24\ \mu\text{m}$ to optical flux ratio implies strong dust heating by the nuclear accreting power source, which is optically blocked by the obscuring dust. Thus, high $24\ \mu\text{m}$ to optical flux ratios (and red $R - K$ colors) can be effective indicators of highly obscured Compton-thick AGNs (e.g., Fiore et al. 2008). Moreover, because the $24\ \mu\text{m}$ to optical flux ratio correlates with the X-ray to optical ratio in AGNs, it can act as an estimator of the relative level of AGN activity and possibly be used to identify low-luminosity and moderately obscured ($N_{\text{H}} \sim 8 \times 10^{22}\ \text{cm}^{-2}$) AGNs (e.g., Georgantopoulos et al. 2008), and thus, megamasers.

In this paper, we investigate the dependences of the H_2O megamaser emission and its properties on the global optical/mid-IR properties of their host galaxies. Identifying such correlations should help us better understand the underlying maser excitation physics while providing new guidance toward optimizing the sample selection criteria for future maser surveys. In Section 2, we describe the samples of maser and non-maser galaxies, and how we collect the associated optical/mid-IR photometric information. We present the general optical and mid-IR properties of our samples and the correlations with the various types of maser emission in Section 3, and we explore the physics of the association of the megamaser emission with obscured AGN activity in Section 4. We summarize the key points of this study and provide guidance for future maser surveys in Section 5.

Throughout this paper, we adopt a Λ CDM cosmology, where Λ denotes the cosmological constant that accounts for DE, and the universe contains cold dark matter (CDM). We adopt $\Omega_m = 0.3$, $\Omega_\Lambda = 0.7$, and $H_0 = 70\ \text{km s}^{-1}\ \text{Mpc}^{-1}$ for the cosmological parameters.

2. The Maser and Non-maser Galaxy Samples and the Optical/Mid-IR Photometric Data

2.1. The Sample

The largest and most comprehensive catalog of all galaxies surveyed for water maser emission at 22 GHz is being compiled and made publicly available by the MCP (Braatz et al. 2010).

Starting in 2005, MCP has conducted maser searches using the GBT with a 1σ rms sensitivity of $\sim 2\text{--}3\ \text{mJy}$ per $24.4\ \text{kHz}$ ($\sim 0.33\ \text{km s}^{-1}$) channel (e.g., Braatz et al. 2004; Braatz & Gugliucci 2008). The redshifts of the galaxies in the GBT surveys are in the range $z = 0.0\text{--}0.07$. The total number of galaxies listed by the MCP Web site by 2016 September is 4863 galaxies. Among the galaxies cataloged by MCP, maser emission is found in 161 galaxies, and the overall maser detection rate is therefore $\sim 3\%$.

We note that while we refer to the data listed on the MCP site as the “MCP samples or catalogs,” they include galaxies that are not the result of MCP surveys. In particular, the following 19 maser galaxies neither are the products of MCP searches nor have been followed-up with GBT as part of the MCP surveys: IC 10, ESO 013-G012, M33, IC 184, IC 342, NGC 2146, VII Zw073, He 2-10, J1028+1046, NGC 3256, NGC 3620, NGC 4038/39, NGC 4214, ESO 269-G012, NGC 4945, NGC 5253, Circinus, NGC 6300, and ESO 103-G35. We also note that the entire sample of galaxies we work with here reflects a simple annexation of all galactic nuclei surveyed in 22 GHz, and that the targeting criteria and sensitivities associated with each constituent survey have not been homogeneous. As a consequence, the overall sample might be affected by (to date, unknown) selection effects; however, none of the photometric measurements considered in this analysis played a major role in selecting these galaxies as potential maser targets.

The data presented in the MCP catalogs comprise sky positions, recession velocities, 22 GHz spectra, the sensitivity of each observation, and the corresponding source brightness temperature. Herein, we refer to galaxies with confirmed H_2O maser emission as maser galaxies or masers, and to galaxies with no maser detection as non-maser galaxies, or non-masers. For the maser galaxies, the MCP catalogs also include the maser luminosities, morphologies (e.g., disk, jet), and the corresponding discovery reference. For those galaxies without available $L_{\text{H}_2\text{O}}$ from the MCP website, we calculate the values based on the GBT spectra. The maser luminosities $L_{\text{H}_2\text{O}}$ are calculated under the assumption of isotropic emission (see Pesce et al. 2015 for the definition). The MCP directory includes also the only two high-redshift galaxies with maser detection: J0804+3607 and J0414+0534 ($z = 0.66$ and $z = 2.64$, respectively). These two sources have strikingly different properties, both in terms of their hosts and in their maser emission, and we do not include them in our analysis. Table 1 lists the general properties of the 161 low- z maser galaxies, including their distances and their water maser luminosities. The distances are estimated by dividing the recession velocities of the galaxies (v_{sys}) by H_0 , when $v_{\text{sys}} \geq 600\ \text{km s}^{-1}$; otherwise, in order to avoid significant distance bias caused by peculiar velocities, we recorded and used here the redshift-independent distances from NED.¹³

2.2. The Classification of Maser Types

For the sample of galaxies with maser detections, we separate them into two general categories based on their isotropic maser luminosities $L_{\text{H}_2\text{O}}$. The low-luminosity category is called “kilomasers,” which comprises 28 galaxies with $L_{\text{H}_2\text{O}} < 10\ L_\odot$. The kilomaser emission is more likely to be associated with star-forming activity rather than an AGN. The

¹³ <https://ned.ipac.caltech.edu>

Table 1
General Properties of the H₂O Maser Galaxies

Galaxy Name	Distance (Mpc)	$L_{\text{H}_2\text{O}}$ (L_\odot)	Galaxy Name	Distance (Mpc)	$L_{\text{H}_2\text{O}}$ (L_\odot)
NGC 23	65.2	180.0	2MASX J11033836-0052081	122.6	26.0
NGC 17	84.7	9.0	2MASX J11093314+2837393	162.3	36.0
2MASX J00114518-0054303	205.5	527.0	NGC 3556	10.0	1.0
2MASX J00272528+4544279	171.5	507.0	NGC 3620	24.0	4.0
IC 10	0.7	0.02	CGCG 185-028	149.4	550.0
NGC 235A	95.2	41.0	NGC 3614	33.3	3.0
NGC 253	3.4	0.2	Arp 299	44.1	125.0
Mrk 348	64.4	400.0	NGC 3735	38.5	20.0
NGC 291	81.5	74.0	CGCG 068-013	152.9	92.0
ESO 013-012	72.1	500.0	NGC 3783	41.7	22.0
2MASX J01094510-0332329 ^a	233.8	1138.0	CGCG 268-089	113.2	149.0
Mrk 1	68.3	50.0	NGC 4038/39	23.5	8.0
NGC 520a	32.4	1.0	2MASX J12020465+3519173 ^a	146.0	520.0
2MASX J01260163-0417564 ^a	80.4	112.0	UGC 7016	103.9	22.0
M33	0.8	0.3	NGC 4051	10.0	2.0
NGC 591 ^a	65.0	25.0	NGC 4151	14.2	0.6
NGC 613	21.1	20.0	NGC 4194	35.7	12.0
IC 184	75.5	20.0	NGC 4214	4.2	0.03
2MASX J02140591-0016371	160.1	74.0	NGC 4253	55.4	9.0
MRK 1029 ^a	129.7	682.0	NGC 4258 ^a	7.2	80.0
NGC 1052	21.0	125.0	NGC 4261	32.0	40.0
NGC 1068 ^a	16.2	160.0	NGC 4293	12.7	1.0
NGC 1106	60.1	8.0	NGC 4388 ^a	36.1	12.0
2MASX J02532956-0014052	124.2	4.0	NGC 4527	24.8	4.0
Mrk 1066 ^a	51.5	32.0	NGC 4633	22.6	0.06
NGC 1194 ^a	58.2	112.0	2MASX J12555984-0804329	57.3	266.0
NGC 1320 ^a	38.0	43.0	ES O269-G012 ^a	71.6	1000.0
2MASX J03364614-0750236	167.5	183.0	NGC 4922B	100.8	200.0
NGC 1386 ^a	12.4	125.0	NGC 4945	8.0	50.0
IRAS 03355+0104 ^a	170.4	227.0	NGC 4968 ^a	42.2	53.0
IC 342	3.3	0.01	NGC 5077	40.1	71.0
2MFGC03185	176.8	3870.0	NGC 5128	7.8	1.0
WISEP J043703.69+245606.9 ^a	69.1	178.0	M51a	7.8	0.6
2MASX J04370825+6637424 ^a	53.9	20.0	NGC 5256	120.3	32.0
IRAS 04385-0828	64.7	43.0	NGC 5253	3.5	1.0
UGC 3157	66.0	85.0	SBS 1344+527 ^a	125.2	379.0
UGC 3193 ^a	63.6	270.0	NGC 5347	33.4	32.0
Mrk 1089	57.4	15.0	2MASX J13553592+0553050	168.0	86.0
CGCG 468-002	75.0	35.0	MCG+11-17-010	137.0	34.0
UGC 3255	81.0	16.0	2MASX J13564736+6937117	150.3	397.0
UGC A116	11.3	3.0	ESO 446-G018	68.2	183.0
Mrk 3	57.9	10.0	UGC 9077	80.4	17.0
NGC 2146	12.8	1.0	NGC 5495 ^a	96.2	600.0
VIIZw073	177.0	137.0	Circinus ^a	4.2	20.0
NGC 2273 ^a	26.3	32.0	NGC 5506	26.5	50.0
ESO 558-G009 ^a	109.6	766.0	MCG-02-37-004	177.7	329.0
UGC 3789 ^a	47.5	370.0	NGC 5643	17.1	25.0
NGC 2410	64.2	14.0	NGC 5691	26.7	4.0
Mrk 78 ^a	159.1	32.0	NGC 5728 ^a	40.0	80.0
IC 485	119.1	1060.0	CGCG 164-019	128.0	30.0
Mrk 1210 ^a	57.8	80.0	NGC 5765b ^a	119.0	2277.0
He 2-10	12.5	0.7	UGC 9618b ^a	144.2	400.0
2MASX J08362280+3327383 ^a	211.6	800.0	UGC 9639 ^a	154.3	444.0
NGC 2639	47.7	25.0	NGC 5793 ^a	49.9	200.0
2MASX J08474769-0022514 ^a	218.2	2210.0	2MASX J15201964+5253560	159.2	44.0
CGCG 120-039	109.8	154.0	UGC 9954	147.4	30.0
2MASX J09053008+0328232	120.3	132.0	2MASX J16070391+0106296	116.7	6.0
NGC 2781	29.3	14.0	IRAS 16288+3929	131.2	16.0
2MASX J09124641+2304273	155.6	143.0	CGCG 168-018	157.4	192.0
NGC 2782	36.6	13.0	NGC 6240	104.8	40.0
NGC 2824	39.4	500.0	NGC 6264 ^a	145.4	2100.0
SBS 0927+493	146.3	280.0	2MFGC13581 ^a	145.6	672.0
UGC 5101	168.6	1900.0	2MASX J17101815+1344058	135.0	69.0

Table 1
(Continued)

Galaxy Name	Distance (Mpc)	$L_{\text{H}_2\text{O}}$ (L_\odot)	Galaxy Name	Distance (Mpc)	$L_{\text{H}_2\text{O}}$ (L_\odot)
Mrk 1419 ^a	70.5	400.0	NGC 6323 ^a	111.0	500.0
NGC 2979	38.9	125.0	NGC 6300	15.8	3.0
NGC 2989	59.2	40.0	CGCG 252-044	105.1	110.0
M82	3.7	200.0	UGC 11035	111.4	291.0
NGC 3081	33.8	17.0	ESO 103-G35	56.9	400.0
NGC 3079 ^a	16.1	500.0	2MASX J19393889-0124328	88.4	160.0
2MASX J10115058-1926436	115.1	371.0	3C 403	252.7	2000.0
NGC 3160	97.9	46.0	NGC 6926 ^a	85.3	500.0
IC 2560 ^a	41.4	100.0	IRAS 20550+1656	154.6	908.0
2MASX J10205956-0010342	239.7	65.0	UGC 11685	83.9	80.0
NGC 3256	40.1	10.0	IC 1361	56.6	35.0
2MFGC08115	191.0	1135.0	2MASX J21445731+1534503	130.5	189.0
UGC 5713 ^a	90.2	237.0	AM 2158-380NED02	142.6	559.0
Mrk 34 ^a	216.3	1000.0	TXS 2226-184	107.1	6300.0
NGC 3359	14.5	0.7	NGC 7479	34.0	19.0
NGC 3393 ^a	53.6	320.0	IC 1481 ^a	87.4	320.0
UGC 6093 ^a	154.7	770.0	MCG+05-55-041	133.7	93.0
CGCG 498-038 ^a	132.0	268.0			

Notes. Columns 1 and 4: name of the galaxy; columns 2 and 5: the adopted distance of the galaxy (see text); columns 3 and 6: the isotropic H_2O maser luminosity. Objects are listed in order of their right ascension.

^a Maser emission in a disk-like configuration; see <https://safe.nrao.edu/wiki/bin/view/Main/MegamaserCosmologyProject> for more details about these maser detections.

higher-luminosity category is called “megamasers,” which includes 132 galaxies with $L_{\text{H}_2\text{O}} \geq 10 L_\odot$. Most of the H_2O megamaser activity is believed to be associated with AGNs; however, starburst activity cannot be ruled out (e.g., the optical spectral classification of $\sim 25\%$ of these galaxy nuclei are consistent with either H IIs or Transition Objects; Constantin 2012).

Within the category of megamasers, we further define a subsample of objects called “disk masers” where the H_2O maser emission exhibits the characteristic spectral pattern of high-velocity features that are redshifted and blueshifted and spatially offset from the features of the systemic velocity (e.g., Herrnstein et al. 1999; Braatz & Gugliucci 2008), or are identified as such from direct mapping of the spatial distribution of the maser emissions using the VLBI technique (e.g., Gao et al. 2016; Kuo et al. 2015). In all of these cases, it is found that the water maser emission originates from the subparsec-scale circumnuclear gas disks at the centers of galaxies (e.g., Herrnstein et al. 1999; Kuo et al. 2011; Gao et al. 2016). This is the only type of maser that allows accurate measurements of BH masses and of the Hubble constant (e.g., Kuo et al. 2013, 2015; Reid et al. 2013; Gao et al. 2016), and is therefore the type of maser system we are most interested in detecting more of. The total number of disk masers identified by this method is 45, and the overall detection rate of such systems is 0.9%. The remaining megamasers are likely to be associated with outflows or jets, or disk masers with blue-shifted/redshifted masers that are too weak to be detected given the sensitivity of our survey; however, the scarce data availability on these cases does not allow us to quantify the real fraction of these situations.

Figure 1 presents a summary of the number statistics of the samples of maser and non-maser galaxies as a function of distance. The left panel shows the normalized distributions of non-masers (dotted–dashed black), masers (dotted yellow), and the subgroups of megamasers (dashed magenta) and disks (continue cyan). ΔN is the number of objects in a given sample in a distance bin, while N is the size of the sample. The right panel shows the detection rates of masers, megamasers, and disks, out of all the galaxies surveyed for water maser emission, as a function of distance. As it is readily apparent from these distributions, the majority of the maser galaxies have been detected within 150 Mpc, and the detection rate decreases with increasing distance. Nevertheless, at distances larger than 50 Mpc, the statistics are not high enough to determine with confidence or quantify the distance dependence.

2.3. Uncertainties in the Maser Detection Rates

The megamaser searches are likely to suffer from variations of the detection limits in terms of their luminosity, because their detection is sensitive not just to the presence of a maser system but also to the flux densities of the individual maser lines. More specifically, detection limits for maser surveys are generally cited in terms of the root-mean-square flux density per spectral channel, and thus, the sensitivity can be restated in terms of the isotropic maser luminosity for a given line width. Since a maser system may consist of many isolated maser components, it is possible that in the case of a maser system with multiple features for which no single channel exceeds the detection threshold, the maser system may remain undetected. Thus, a maser survey with a uniform luminosity limit is not feasible, and there is no practical way to estimate the number of missing maser systems in a given distance (or other parameter)

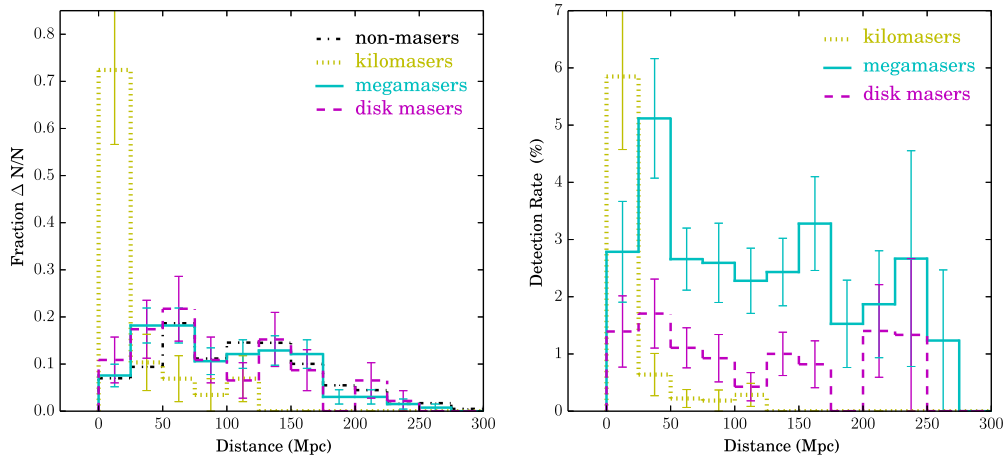


Figure 1. Left panel: normalized number of masers and non-masers in the MCP sample as functions of distance. Right panel: the maser detection rates as a function of distance. The error bars illustrate the associated Poisson uncertainties.

range. As a consequence, the errors associated with the maser detection rates cannot account for this effect.

We also want to emphasize that what we call “detection rate” is simply defined as the fraction of objects that are detected in 22 GHz emission from all of the objects surveyed for this kind of emission, in the respective bin of host properties, and therefore it simply reflects the number of all systems above the detection threshold, regardless of how luminous these sources are in their 22 GHz activity, or in what cosmic volume they have been detected. We point out that we do not (and are not yet able to) estimate or calculate the true prevalence of maser emission in host galaxies with certain properties.

On the other hand, there are additional uncertainties that could particularly affect histogram comparisons (e.g., Figure 1). Specifically, the values we list and compare in (any) histograms are subject to uncertainties in the values that are being binned up to create the histogram (i.e., the bin-hopping effect). We checked, however, these effects on the validity of the conclusions based on the histogram comparisons throughout this study by employing comparisons of histograms built by bootstrapping, i.e., adding/subtracting objects from various bins and placing them in the adjacent ones, and we did not identify any significant change. In particular, using a simple Monte Carlo (MC) approach, we create the same histogram many times, each time replacing each data point by a new one drawn from the distribution corresponding to that data point’s uncertainty (i.e., a Gaussian with a mean equal to the data point’s value and variance equal to the square of its uncertainty). By generating a large number of these histograms and looking at the root mean square of the value within any particular bin, we are able to get a very robust estimate of the “bin-hopping” uncertainty allowed by the data set. Such a technique has the added benefit of also determining the “most likely” value for the histogram bin itself, by averaging the values we get from the MC process. We find that the result of adding uncertainty to the measurements is to (1) smooth out the overall shape of this histogram, and (2) increase the value of the error bar in any single bin. However, for this particular sample and its subgroups, the Poisson uncertainties remain dominant.

2.4. Optical Photometry of the Galaxy Samples

The optical photometric data for our MCP samples come primarily from the SDSS (York et al. 2000; Abazajian et al. 2009;

Ahn et al. 2014), and we adopt the SDSS u , g , r , i , z magnitude values reported in the NASA/IPAC Extragalactic Database (NED). Out of the total MCP sample of 4863 galaxies, NED provides SDSS magnitudes for 2753 galaxies (i.e., 57% of the sample). Among these galaxies, 2731 of them have various types of SDSS magnitudes coming from different model fittings (i.e., PSF, Model, CModel, Petrosian¹⁴). We adopt here the “Model” magnitudes, which provide good estimates of the global galaxy fluxes independent of aperture sizes. For the rest of the 32 nearby galaxies where “Model” photometry is not available (the SDSS catalog is missing many nearby, bright galaxies because of the difficulty of automatic photometric processing of big galaxies), NED provides SDSS photometry from observations with aperture sizes large enough to cover the bulk of the galaxy except for seven systems (NGC 3521, NGC 3627, NGC 4631, NGC 4826, F15327+2340, NGC 6269, and NGC 7331). We exclude these galaxies from the statistical analysis that involves optical photometric properties.

Among the 2749 galaxies with available SDSS photometry, there are 63 megamaser detections, among which 18 show a disk-like configuration. Thus, in terms of optical photometry, the overall detection rate of all masers, megamasers, and disk masers are therefore 2.3%, 1.9%, and 0.7%, respectively. These values are slightly lower than those of the whole MCP sample in the same ratio, however, implying that selection biases that generally affect the various maser-type detection efficiency should not be significantly different for the subset of galaxies with SDSS photometry. Nonetheless, any comparisons between the entire MCP and the SDSS-MCP samples should be made with some caution because the two samples may have some intrinsic differences in terms of galactic properties.

2.5. Mid-infrared Photometry of the Galaxy Samples

We collect the mid-IR photometric data of our MCP samples entirely from the public all-sky source catalog provided by *WISE* (Wright et al. 2010) via the NASA/IPAC Infrared Science Archive¹⁵ using the IRSA¹⁶ catalog tool. *WISE* mapped the sky at 3.4, 4.6, 12, and 22 μm ($W1$, $W2$, $W3$, $W4$) in 2010 with an

¹⁴ See <http://www.sdss.org/dr12/algorithms/magnitudes/>.

¹⁵ <http://wise2.ipac.caltech.edu/docs/release/allsky/>

¹⁶ <http://irsa.ipac.caltech.edu/Missions/wise.html>

angular resolution of $6''.1$, $6''.4$, $6''.5$, and $12''.0$ in these four bands, respectively.

Our cross-matching technique searches for all *WISE* detections within an initial cone search radius of $2''$, with a gradual increase of the search radii of up to $10''$, with a step size of $0''.5$. For comparison, the GBT beam size at 22 GHz is $\sim 30''$. We require all of the MCP-*WISE* matches to be positioned within $10''$ from the GBT source positions and to be detected at better than 3σ in both the 3.4 and $4.6\ \mu\text{m}$ bands (*W1* and *W2*, respectively), which are used to identify and classify these galaxies as AGNs based on the *W1* – *W2* color (see Section 3.2.1, Figure 3). We also require for the matches to have signal-to-noise ratios of $S/N \geq 3$ in the *W4* band. We did not restrict the detection S/N in the *W3* band because galaxies that meet our requirements in *W4*, which is the least sensitive band, will generally have higher S/N detections in the *W3* band. For all duplicates and search radii larger than $6''$, we visually inspected the *WISE* matches in all four *WISE* bands to make sure that it corresponds to the MCP source. The proximity of all these galaxies allows unambiguous detections for the great majority of our sources (86% of the entire sample; 4174 galaxies) in all four passbands; all of the kilomasers and megamaser disks are found to have a *WISE* counterpart while the megamasers only have a 98% *WISE* match.

Overall, the overlap with *WISE* is higher than that with optical photometry, allowing for a greater statistical significance of the investigation of the mid-IR features that may link to the masing activity in galaxy centers. The high MCP-*WISE* matching rate for the megamasers and disks is somewhat expected, if not encouraging, since these systems are expected to have strong mid-IR emission and therefore highly detectable counterparts given the previously proposed scenarios for maser emission associated with the circumnuclear dusty torus in AGNs, which (re)emits in the mid-IR regime. Nevertheless, accounting for the maser selection bias (as being targeted out of Seyfert galaxies; Constantin 2012), it is important to investigate whether the maser-Seyferts differ from other Seyferts in their mid-IR emissions due to properties related to the maser emission.

3. Results: The Observed Correlations

3.1. Optical Photometric Properties of Maser Galaxies

Optical photometric measurements have been relatively successfully employed in the past for mapping the distribution of galaxy properties that can be used to constrain semi-analytic models of galaxy formation evolution processes. Here we briefly address the degree to which the presence and strength of maser emission in galaxy centers relate to the optical colors and absolute brightness of their hosts.

To compare the colors of maser and non-maser galaxies, we consider the *u* – *r* color, which is sensitive to extinction, as well as to the UV flux and the 4000 Å break, and thus relates to the age and properties of the associated stellar populations. For the absolute brightness, we are considering the *g*-band absolute magnitude M_g , which is converted from the observed SDSS *g* magnitude. We note that the trends found here with M_g are consistent with those exhibited when other SDSS magnitude bands are used. To compute colors, we use extinction (Schlegel et al. 1998) and *K*-corrected model magnitudes.

For a very basic comparison of their morphological properties, we examine the distribution of inverse concentration

indices (ICIs) measured by the SDSS photometric pipeline (Lupton et al. 2001; Stoughton et al. 2002; Pier et al. 2003). ICI is defined by the ratio $ICI = r_{50}/r_{90}$, where r_{50} and r_{90} correspond to the radii at which the integrated fluxes are equal to 50% and 90% of the Petrosian flux, respectively. A small ICI value corresponds to a relatively diffuse galaxy and a large ICI value to a highly concentrated galaxy. The concentration index (or the ICI) has been shown to correlate well with galaxy type (Shimasaku et al. 2001; Strateva et al. 2001).

We show in Figure 2 the distribution of the MCP galaxy samples in the *u* – *r* color and M_g , together with the maser detection rates for each subcategory of maser (kilomasers, megamasers, and disk masers), as a function of these two parameters and as a function of ICI. In the color-magnitude diagram, the yellow triangles, cyan squares, and magenta filled circles represent the kilomasers, megamasers, and disk masers, respectively; the sample of non-masers are shown in gray bullets. We are using the same symbol and color scheme to label different types of masers throughout the rest of the paper.

These plots show that different types of maser galaxies have substantially different distributions in the color-magnitude diagram. In particular, the megamasers tend to be brighter than the kilomasers: 83% of megamasers lie above $M_g = -19.7$ while only 18% of the kilomasers exhibit this level of optical brightness. The disk megamasers reside 100% in these optically brighter galaxies as they all have $M_g < -19.7$. These trends are consistent with the findings of Zhu et al. (2011) who considered *B*-band absolute magnitudes derived from SDSS photometry.

The preference of megamasers and disk masers to lie in galaxies with $M_g < -19.7$ is interesting in light of the findings of Kauffmann et al. (2003) who show that among nearby galaxies, the $M_g \sim -20$ mag (corresponding to the stellar mass $\sim 3 \times 10^{10} M_\odot$) marks a transition point beyond which there is a rapid increase in the fraction of galaxies with old stellar populations, high surface stellar densities, and high stellar concentrations typical of bulges. The trends we find here suggest then that the megamasers prefer optically bright hosts with likely higher stellar masses. A direct comparison of the dependence of the maser emission properties on stellar characteristics indicators like those used by Kauffmann et al. (2003) is, however, only possible for a small fraction of our sample (44/162 maser galaxies have SDSS spectroscopy), and a preliminary analysis reveals a possible trend toward more massive (and younger) stellar populations, however, at a weak statistical significance (e.g., Constantin 2012).

In terms of the maser detection rates, we see a clear increase with higher (lower) M_g values for the disks and possibly for the whole subsample of megamasers, whereas the trend may be the opposite for kilomasers. Nevertheless, despite the fact that the detection rate of megamasers is enhanced at lower M_g by up to $\sim 4\%$, the improvement based on the optical photometry alone is too small to be useful for future maser survey. Nonetheless, as we will show in Section 3.3.5, when used in conjunction with mid-IR photometric information, optical photometry becomes quite useful for producing a significant increase in maser detection.

On the other hand, the maser detection rate for different maser types reveals a rather weak dependence on the galaxy color, suggesting that megamasers do not prefer to reside in a particular type of galaxy; while the disks appear to occupy the *u* – *r* > 2.22 locus, there is a small fraction of megamasers

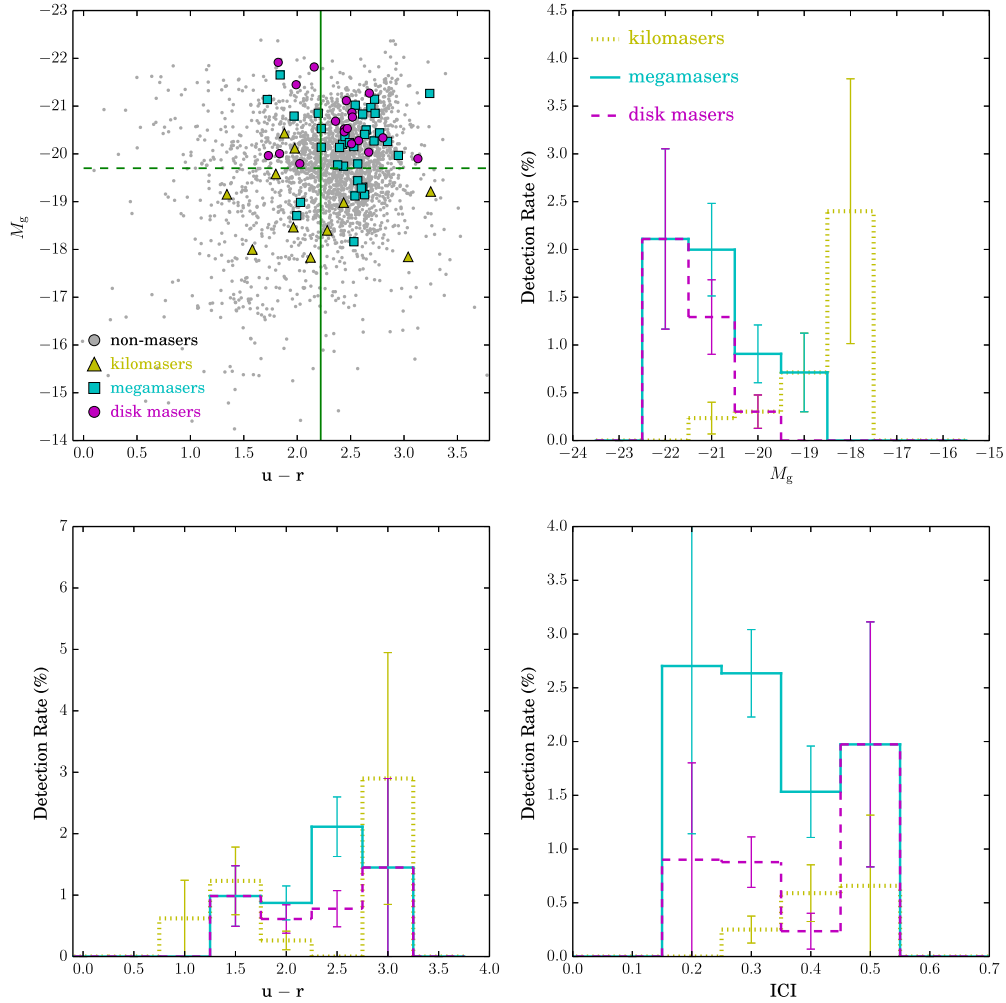


Figure 2. Upper-left panel: the distribution of the sample galaxies in absolute g magnitude (M_g) and $u-r$ color. The kilomasers are shown as filled yellow triangles, megamasers as cyan squares, disks as magenta filled circles, and non-masers as small gray circles. The horizontal and vertical dashed lines correspond to $M_g = -19.7$ and $u-r = 2.2$, respectively. Upper-right panel: the maser detection rates as a function of M_g . The kilomasers, megamasers, and disk masers are shown with the dotted yellow, solid cyan, and dashed magenta lines, respectively. The errors correspond to the Poisson uncertainties of the maser detection rates in each bin. Lower-left panel: the maser detection rates as a function of the $u-r$ colors; $u-r > 2.22$ suggests early-type galaxies (E, S0, and Sa) while $u-r < 2.22$ suggests late-type galaxies (Sb, Sc, and Sd). Lower-right panel: the maser detection rates as a function of the inverse concentration index.

(1.3%) with bluer colors. Given that the $u-r = 2.22$ color can be used to separate early- (E, S0, and Sa) and late-type (Sb, Sc, and Sd) galaxies (Strateva et al. 2001), and that the majority of our maser galaxies with $u-r > 2.22$ are early-type spirals rather than ellipticals, it is possible that our conclusions apply to spiral hosts only. On a similar note, the ICI parameter does not prove to be useful in delineating megamasers or disks, as their detection rates does not show any particular enhancement for any range; the kilomasers, however, do appear to prefer galaxies with higher ICI values, which, as expected in these cases, are associated with late-type hosts.

3.2. Mid-infrared Properties of Maser Galaxies

An association of the maser activity with AGN emission is plausible; however, it is by no means clear how the obscuring torus and the masing disk are related. We do not know yet whether megamaser disks are always related to black hole accretion, or whether they require a dusty/molecular torus. If this torus is necessary for strong maser disk emission, would

the properties of the dusty torus be similar or different among all megamaser disks? Would they reflect similar or different temperature ranges, and thus different mid-IR SEDs and colors? Would any similarities or differences in their mid-IR SEDs help us build more efficient maser disk surveys? We explore these connections in the following subsections.

3.2.1. $W1 - W2$ versus $W2 - W3$

Previous studies found that we can detect a large portion of the population of red/dusty AGNs that do not show AGN-like optical signatures by using the *WISE* $W1 - W2$ versus $W2 - W3$ color diagrams. Mid-IR color cuts proposed for selecting red/obscured AGNs include $W1 - W2 \geq 0.5$ (Satyapal et al. 2014), $W1 - W2 \geq 0.8$ for a lower contamination by non-active galaxies (Stern et al. 2012), and sets of criteria involving both of these *WISE* colors, with even more stringent control for non-AGN contamination (e.g., Jarrett et al. 2011; Mateos et al. 2012). Figure 3 illustrates in the left panel the location of all of our MCP objects in the ($W1 - W2$, $W2 - W3$) color-color

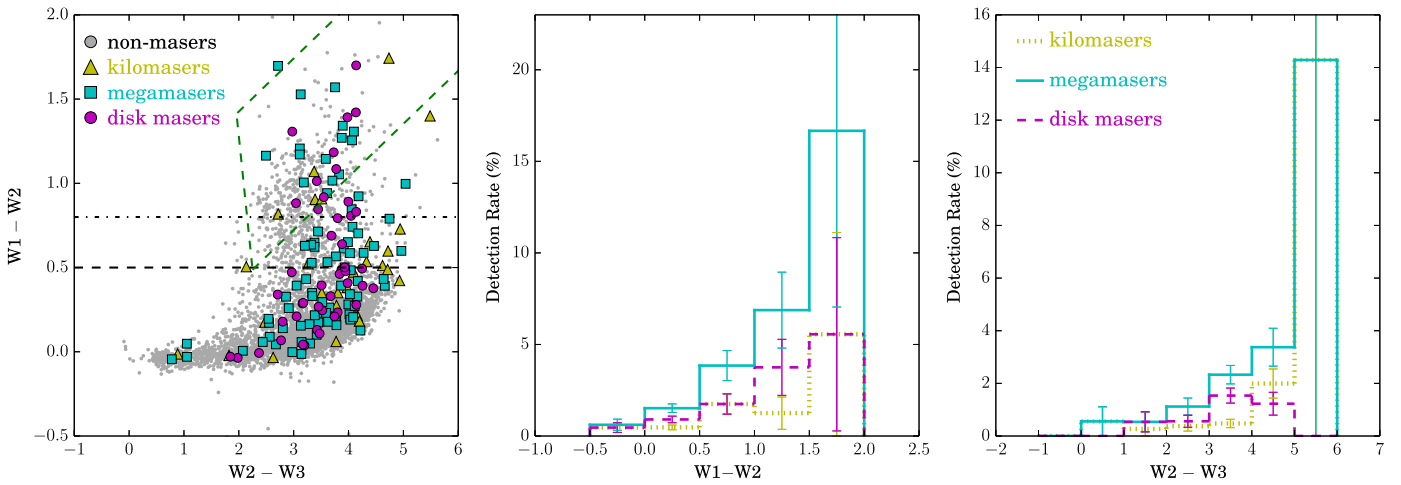


Figure 3. Left panel: the distribution of the MCP samples of maser and non-maser galaxies in the $W2 - W3$ vs. $W1 - W2$ diagram. The horizontal dashed and dotted-dashed lines correspond to the $W1 - W2 = 0.5$ and $W1 - W2 = 0.8$ cuts, respectively. The green dashed line illustrates the wedge defined by Mateos et al. (2012). Middle and right panels: the maser detection rate as a function of $W1 - W2$ and $W2 - W3$.

space, along with these *WISE*–AGN cuts. We chose to work with the Mateos et al. (2012) wedge cut here and note that the results are very similar if the Jarrett et al. (2011) box is used instead.

If there is a strong association between megamaser and disk emission and obscured AGN activity, then we expect to see most of these systems with *WISE* colors of $W1 - W2 \geq 0.8$ or within the Mateos et al. (2012) wedge, with most of the non-masars falling below the $W1 - W2 = 0.5$ line. It seems, however, that this is not immediately the case: the masers and non-masars occupy color–color regions that overlap considerably. The distributions of both maser and non-maser galaxies follow the expected spread of galaxies (Wright et al. 2010), without a clear delineation of *WISE* galaxy colors that can be associated with the masers. The only possible difference is in their average $W2 - W3$ color, which is clearly redder for the masers ($\langle W2 - W3 \rangle$ is 3.51 ± 0.06 for all masers and 3.07 ± 0.01 for non-masars). Only 24% and 42% of maser galaxies satisfy the criteria $W1 - W2 \geq 0.8$ and $W1 - W2 > 0.5$, respectively, while only 18% of maser galaxies fall within the color wedge defined by Mateos et al. (2012). Among megamasers and disks, only $\sim 1/3$ fall into the red *WISE* AGN category, regardless of which criteria are used, which implies that the majority of the disk megamasers are not necessarily associated with obscured dominant AGN activity.

Interestingly, while these mid-IR criteria for selecting obscured AGNs do not seem to be particularly useful in finding a large fraction of megamasers and disks, the overall maser detection rates skyrocket in the red *WISE* AGN regime. We show the maser, megamaser, and disk detection rates as a function of these two colors in the central and right panels of Figure 3. Overall, maser emission is detected among $\sim 9\%$ of these sources, with a high proportion of them being megamasers and disks; there is a significant increase in the expected megamaser and disk detection (7%–9% and 2%–3%, respectively, depending on the color criteria), which represents a boost by at least a factor of 3 from the currently low rate of $< 3\%$ and $< 1\%$, respectively. Thus, these trends also suggest that red AGNs are more likely to host a powerful water maser than bluer AGNs.

Thus, while within the whole population of nearby galaxies there are very few objects with red $W1 - W2$ colors ($\sim 4\%$;

Stern et al. 2012), it is definitely of great value to study these systems carefully, and definitely to survey them all for maser emission. However, it is also clear that we will only recover about a third of the whole population of megamasers within this color regime. It is thus of interest to try to understand what other properties could be used to distinguish between masers and non-masars, especially within the *WISE* blue galaxy population as well.

3.2.2. The Role of the Mid-IR Absolute Brightness

After studying the role of the red AGN-sensitive $W1 - W2$ and $W2 - W3$ colors in detecting maser galaxies and their subtypes of megamasers and disks, we extend our exploration to all possible mid-IR information that can be provided by the *WISE* observations. Among all of the available mid-IR information for these galaxies, we find that the absolute mid-IR magnitudes (M_{W1} , M_{W2} , M_{W3} , M_{W4}) convey important messages for enhancing the water maser detection rates. We discuss here the most significant trends.

Figure 4 shows the distribution of our sample of maser and non-maser galaxies in the (M_{W1}, M_{W3}) and (M_{W2}, M_{W4}) diagrams, as well as the average mid-IR SEDs (average νL_ν values calculated for each *WISE* band, plotted as a function of each band’s central wavelength) per maser type. The *WISE* fluxes for each galaxy have been calculated using the magnitude to flux conversion method described in Wright et al. (2010), and the luminosities were calculated using the distances listed in Table 1.

The most prominent trend that this comparison reveals is that the megamasers are significantly brighter than both the non-masars and the kilomasers in all of the four *WISE* bands. In fact, the mid-IR absolute luminosities or absolute magnitudes appear to be an efficient separator between kilomasers and megamasers, with the latter being, on average, at least one order of magnitude more luminous (see right panel of Figure 4). Galaxies without a detected maser emission exhibit average absolute luminosities (or magnitudes) in between those of kilomasers and megamasers. When the average integrated mid-IR luminosities L_{MIR} are calculated, the trends remain equally obvious: $\langle L_{\text{MIR}} \rangle_{\text{kilomasers}} = 1.7 \times 10^{43} \text{ erg}^{-1}$ while

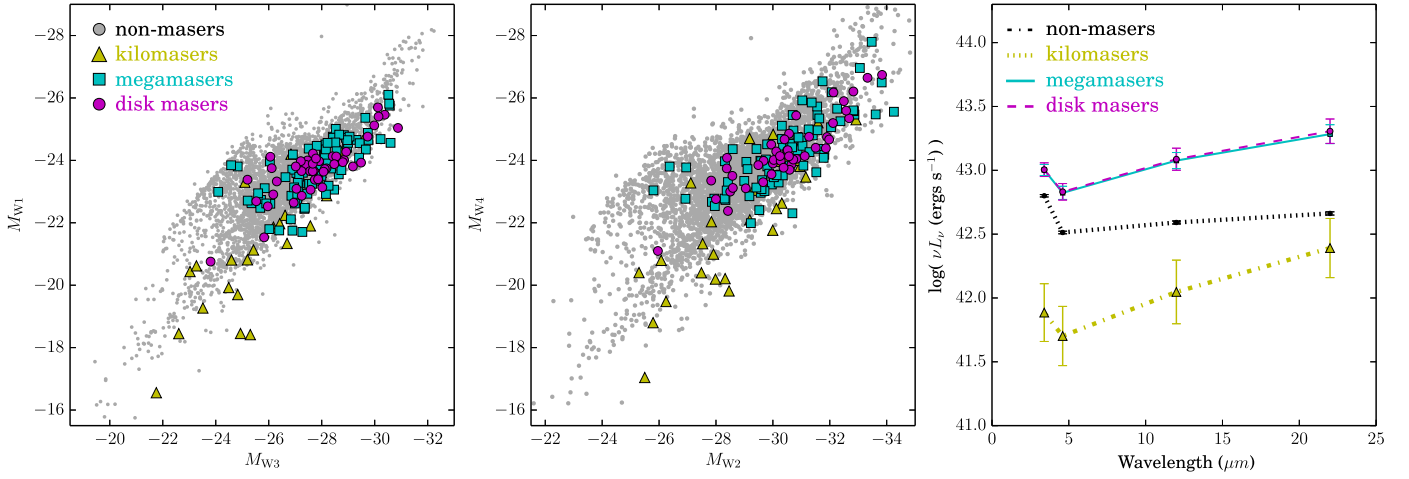


Figure 4. Left and middle panels: the distribution of the MCP galaxies in the (M_{W3}, M_{W1}) and the (M_{W2}, M_{W4}) parameter space. M_{W1} , M_{W2} , M_{W3} , and M_{W4} are the absolute magnitudes of the *WISE* bands. Right panel: average νL_ν values as a function of the *WISE* mid-infrared wavelengths for the MCP kilomasers (yellow triangles), megamasers (cyan squares), disks (magenta filled circles), and non-masars (small gray circles).

$\langle L_{\text{MIR}} \rangle_{\text{megamasers}} = 1.4 \times 10^{44} \text{ erg}^{-1}$. The megamasers and their subgroup of disks remain similar in their mid-IR total power output; however, it is important to note that the object with the highest luminosity in each of the four *WISE* bands is a disk-maser galaxy (NGC 1068). By comparison, the least mid-IR luminous maser is a kilomaser (M33). Thus, targeting more mid-IR luminous galaxies is bound to return a higher fraction of megamaser-emitting systems in general, and megamaser disks in particular.

These differences may suggest that dust heating is more significant in masers than in nonmasers, and the heating process might be either proceeding more efficiently or simply be quantitatively more enhanced in these sources. Unfortunately, the average SED shapes do not offer a clear way of breaking this degeneracy; they simply reveal a clear difference between the masers and non-masers, with the latter having a significantly flatter SED in the longer mid-IR wavelengths, i.e., less reprocessing by the dust; the slightly red average slopes we measure for the megamasers are not statistically significantly different, which is consistent with the comparisons of average *WISE* colors presented above. Nevertheless, the kilomasers are usually associated with star-forming regions (Lo 2005; Ott et al. 2013), and thus, for very similar mid-IR colors or SED slopes, the order of magnitude more power exhibited by megamasers is highly suggestive of an additional radiation source, e.g., an AGN.

Additionally, this comparison also suggests that $W1 - W4$ could also be exploited as a separator between masers and non-masers. Because the *W4* band is the most luminous in megamasers, especially for the disks, and is thus the wavelength region where the mid-IR emission peaks, the $L_{W4} = \nu L_\nu$ estimated at $22 \mu\text{m}$ can be an effective tool to explore for picking up the additional mid-IR photons from the heated dust that is directly associated with the maser emission. Indeed, when we compare the megamaser and disk detection rates in all four *WISE* bands, we find that they correlate best with L_{W4} . We present in the following section a detailed analysis of the dependence of the maser properties on the $W1 - W4$ color and show that it can be efficiently used as a measure of obscured AGN activity in galaxy centers.

3.3. Combining the Optical and Mid-IR Information

We are exploring here ways in which combinations of the optical and mid-IR photometric measurements and results presented in the previous sections can be best exploited to identify the closest links between maser emission and their host properties, and thus to enhance the megamaser detection rates.

3.3.1. $W1 - W4$ as a Proxy for the $f_{24 \mu\text{m}}/f_r$ Flux Ratio

As mentioned in Section 1.3, the $24 \mu\text{m}$ to optical ($f_{24 \mu\text{m}}/f_r$) flux ratio of type 2 AGNs is well correlated with the X-ray-to-optical flux ratio, which makes the former parameter a good diagnostic for the “relative” level of obscured AGN activity (Fiore et al. 2008; Georgantopoulos et al. 2008; Rovilos et al. 2011). Because the optical flux of a galaxy can be converted to stellar mass (M_*) by assuming a universal initial mass function (Kauffmann et al. 2003), and the X-ray flux can be used to estimate the total luminosity of an AGN (L_{AGN}) by adopting a certain bolometric correction, the X-ray-to-optical flux ratio is then a measure of the L_{AGN}/M_* ratio or the specific black hole accretion rate λ_{SBHAR} . This ratio can also measure the rate of the black hole accretion normalized (or relative) to the host stellar mass (Aird et al. 2017; Georgakakis et al. 2017). It has been argued that λ_{SBHAR} is a more fundamental property of an AGN than the observed luminosity, and that, under certain assumptions, λ_{SBHAR} can be a proxy for the Eddington ratio (e.g., Aird et al. 2017).

Because of the concurrence of the *W4* band with the $24 \mu\text{m}$ emission, the $r - W4$ color is a great proxy for the $24 \mu\text{m}$ to optical flux ratio. With the goal of exploring the widely available *WISE* photometry for our MCP sources, and because the *W1* band is the closest *WISE* band to the optical *r* band, we explore here the relationship between $r - W4$ and $W1 - W4$, and thus, the potential use of $W1 - W4$ as a measure of the “relative” level of obscured AGN activity.

We show in Figure 5 the distribution of all MCP galaxies with available SDSS *r*-band measurements in the $r - W4$, $W1 - W4$ color-color diagram (left panel), along with the standard deviations of $W1 - W4$ in each $r - W4$ bin (middle panel), and the detection rates of the various subtypes of masers as a function of $W1 - W4$ (right panel). It is quite apparent that $r - W4$ and $W1 - W4$ correlate strongly (the Spearman’s rank

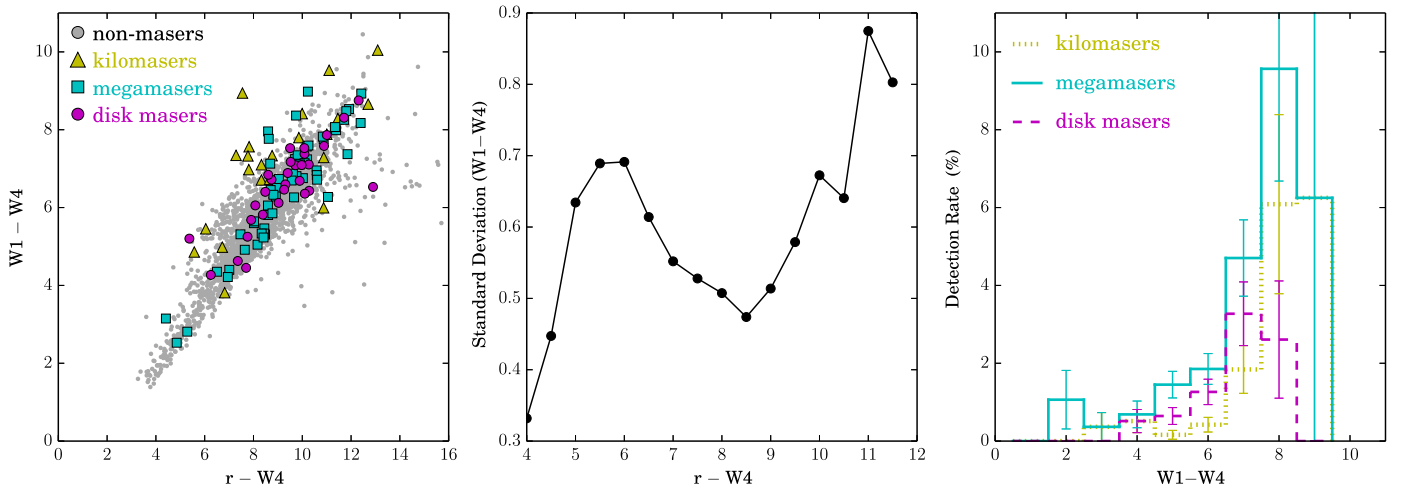


Figure 5. Left panel: the distribution of the MCP galaxies in the $(r - W4, W1 - W4)$ parameter space. The Spearman rank correlation coefficient between $r - W4$ and $W1 - W4$ is 0.86. Middle panel: the standard deviation of $W1 - W4$ as a function of $r - W4$. Right panel: the kilomaser, megamaser, and disk detection rates as a function of $W1 - W4$.

correlation coefficient is 0.86, and the standard deviations average at 0.6 and do not exceed 0.8) for the whole MCP sample. The correlation is only slightly weaker statistically when the kilo/mega/disk-maser samples are considered separately, with the Spearman’s rank correlation coefficient dropping to 0.6.

The high degree of correlation of $r - W4$ with $W1 - W4$ suggests that $W1 - W4$ can act as an indicator of the level of the true AGN activity or the specific black hole accretion rate. Under the assumption that the megamaser and the AGN activities are linked, this new tool should then offer significant improvements in the maser detection rates since only about half of our MCP sample has SDSS photometry while the $W1 - W4$ color is measurable for nearly all of these objects. Moreover, the maser detection rates, for all types of maser galaxies, are clearly increasing with redder $W1 - W4$ values, easily reaching greater than 5% levels for $W1 - W4 > 6$, which translates into a boost of a factor of 2–4 relative to the current detection rates. Additionally, the nearby galaxies with $W1 - W4 > 6$ account for 43% of the total population, which corresponds to an improvement of a factor of 3 (or 5) in the size of the potential parent target population when compared to the number of galaxies with $W1 - W2 > 0.5$ (or $W1 - W2 > 0.8$), regardless of the availability of SDSS photometry. Thus, $W1 - W4$ has the potential to help substantially enlarge the sample size for studying the dependence of maser emission and its properties on the level or type of the associated AGN activity.

3.3.2. $W1 - W2$ versus $W1 - W4$

Now, if $W1 - W2 \gtrsim 0.5$ is effective for finding red/obscured AGNs and a high fraction of masers, and since $W1 - W4$ proves to be an adequate tool for picking up sources with a high “relative” level of obscured AGN activity and also maser galaxies, it is of great interest to look into what these two colors can provide us with when used together. We show in Figure 6 the distribution of the MCP galaxies in these two parameters.

This plot primarily reveals that in the region where $W1 - W2 \gtrsim 0.5$, adding the extra dimension of $W1 - W4$ can effectively separate maser galaxies from non-maser galaxies. If we select a sample by using the criteria

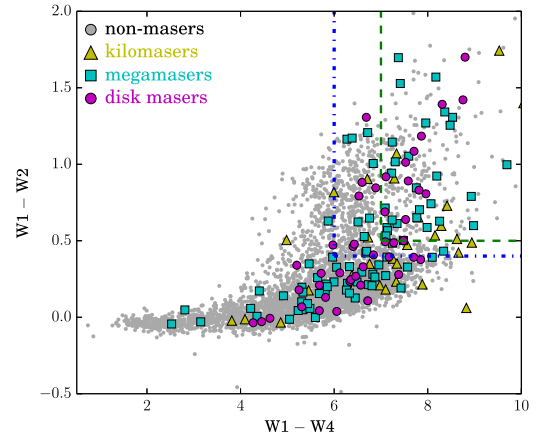


Figure 6. The distribution of the MCP galaxies in the $(W1 - W4, W1 - W2)$ color-color diagram. The green dashed lines correspond to $W1 - W2 = 0.5$ and $W1 - W4 = 7$. The overall maser detection rate for sample galaxies having $W1 - W2 > 0.5$ and $W1 - W4 > 7$ is $18\% \pm 3\%$, while megamasers and disks are expected to be detected at the impressive rates of $\sim 15\%$ and $\sim 5\%$, respectively. A more relaxed constraint of $W1 - W2 > 0.4$ and $W1 - W4 > 6$ (shown with blue dotted-dashed lines) still recovers high detection rates of 11%, 9%, and 3% for the overall maser population, the megamasers, and the disks, respectively, with a 50% increase in the completion rates.

$W1 - W2 > 0.5$ and $W1 - W4 > 7$, the maser detection rate can be boosted to $18\% \pm 2\%$, which is ~ 6 times higher than the current maser fraction (3%). Interestingly, the overall maser detection rate does not show a further increase when tighter selection criteria (e.g., $W1 - W2 > 0.8$) are considered. Hence, 18% is about the maximum detection rate one can achieve, and that is obtained by using $W1 - W4$ and $W1 - W2$ to select maser-emitting systems. In terms of megamasers and their subgroup of disks, the detection rates associated with these criteria become $15\% \pm 2\%$ and $5\% \pm 1\%$, respectively, which constitute impressive ~ 5 times higher rates than the current values.

These rather dramatic increases in the maser detection rates are, however, shadowed by a relatively small pool of potential target galaxies, which translates into a high likelihood of missing a large fraction of megamasers and disks (only 32% and 28% of all megamasers and disks, respectively, fall under

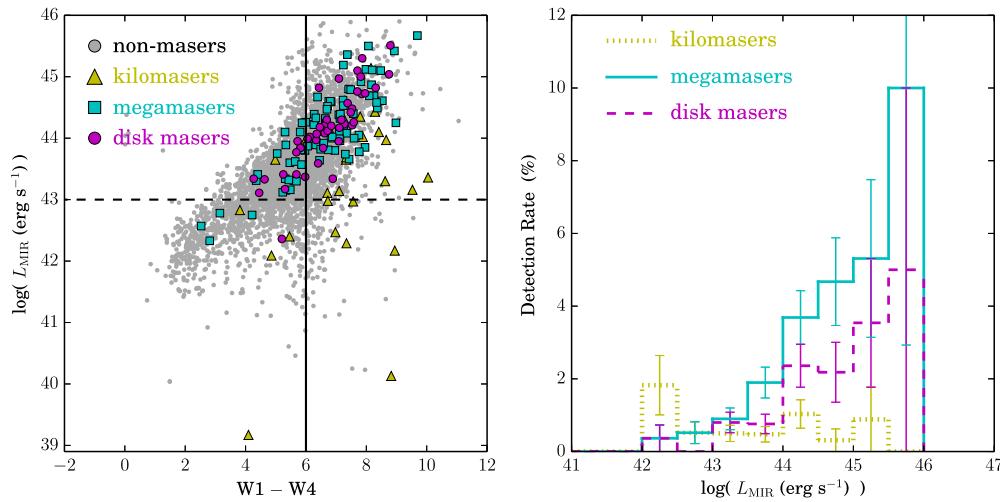


Figure 7. Left panel: the distribution of MCP galaxies in L_{MIR} and $W1 - W4$. The Spearman-rank correlation coefficients are 0.67, 0.29, and 0.82 for the samples of all MCP objects, the kilomasers, and the megamasers, respectively. Right panel: the maser detection rates as a function of L_{MIR} .

these criteria). Maybe not surprisingly, not all of the 18% galaxies expected to exhibit red *WISE* colors of $W1 - W2 > 0.5$ show $W1 - W4 > 7$, leaving only 11% of all galaxies in this parameter range. Nevertheless, a slight relaxation of these constraints to $W1 - W2 > 0.4$ and $W1 - W4 > 6$ (shown in Figure 6 with blue dotted-dashed lines) increases the parent target population to 17%, and still recovers high detection rates of 11%, 9%, and 3% for the overall maser population, the megamasers, and the disks, respectively. The sample completion rates are also increased by 50%, meaning that the likelihood of losing good megamasers (i.e., disks) is significantly diminished. Thus, these criteria offer a very effective balance between high maser detection and completion rates among selections based on optical classifications or mid-IR photometry, making this way of selecting maser targets the most promising for great enhancements in maser detections in future surveys.

3.3.3. The Combined Effect of L_{MIR} and $W1 - W4$

Because a significant portion of the total AGN luminosity in obscured AGNs is re-emitted in mid-IR wavelengths, if the strength of the AGN activity plays a role in exciting the maser emission, one might expect a correlation between the megamaser detection rate and their host's total mid-IR luminosity L_{MIR} . We explore this in Figure 7, where we show the distribution of the MCP galaxies in the L_{MIR} and the $W1 - W4$ color, along with the detection rates of various maser types as a function of L_{MIR} .

Interestingly, while there is no obvious strong correlation between L_{MIR} and $W1 - W4$ for the whole MCP sample or for the subsample of kilomasers, when only the megamasers are considered, the two mid-IR measures become rather tightly correlated: the Spearman rank coefficients are 0.67, 0.29, and 0.82 for the samples of all MCP objects, the kilomasers, and the megamasers, respectively. Since $W1 - W4$ can be an indicator of AGN strength (see Section 3.3.1), the correlation between L_{MIR} and $W1 - W4$ for megamasers suggests that the mid-IR luminosity can also be employed to estimate the level of AGN activity, and thus, to enhance the maser detection rate. Indeed, the megamaser and disk detection rates show a significant increase toward higher L_{MIR} , with levels above

5% for $L_{\text{MIR}} \gtrsim 10^{43} \text{ erg s}^{-1}$, where the kilomaser presence starts diminishing (Figure 7, right panel).

We note that this potential threshold in L_{MIR} for megamaser detection is reminiscent of the results of Zhu et al. (2011), who show that the maser detection rate increases as a function of the [O III] luminosity, which is considered to be an important tracer of the bolometric luminosities of AGNs. Thus, the increasing maser fraction as a function of mid-IR luminosity brings additional support to the scenario that the AGN strength plays a significant role in exciting maser emission.

In addition to strengthening the link between megamaser and AGN activities, this plot also indicates that the megamaser detection rate can be additionally boosted by at least a factor of ~ 2 by selecting galaxies with $L_{\text{MIR}} \geq 10^{44} \text{ erg s}^{-1}$, to $6.7\% \pm 0.8\%$ and $2.5\% \pm 0.5\%$ for megamasers and disks, respectively. Furthermore, as we argue in the next subsections, by combining these trends with those in optical photometry, we can improve the odds of finding megamaser disks even further.

3.3.4. The Combined Effect of L_{MIR} and $u - r$

We recall that while the $f_{24 \mu\text{m}}/f_r$ flux ratio in itself does not measure the AGN activity, the ratio can be used to estimate the level of AGN emission relative to that of the host (therefore, as discussed before, the relative level of AGN activity); thus, it is the enhancement in this ratio that reflects the strength of the putative AGN. We also note that the $f_{24 \mu\text{m}}/f_r$ ratios among normal galaxies (i.e., without a dominant AGN) exhibit an intrinsic range that is highly dependent on the galactic morphology (e.g., Rovilos et al. 2011), with later types (of bluer optical colors) exhibiting higher intrinsic $f_{24 \mu\text{m}}/f_r$ ratios than galaxies with earlier morphologies (of redder optical colors). Thus, for a certain population of galaxies sharing the same (or no) level of AGN activity, the $f_{24 \mu\text{m}}/f_r$ ratios increase as the galaxy colors change from red to blue without mirroring a significant (optically detected) AGN enhancement.

We showed that the megamaser activity is more enhanced (i.e., higher megamaser detection rates) for stronger mid-IR emitters (higher L_{MIR} values), and with redder $W1 - W4$ colors (Section 3.3.3, Figure 7), which also correlate well with higher $f_{24 \mu\text{m}}/f_r$ ratios (Section 3.3.1, Figure 5), while there is no significant correlation with the optical $u - r$ color, and thus with the host morphology (Section 3.1, Figure 2). A natural

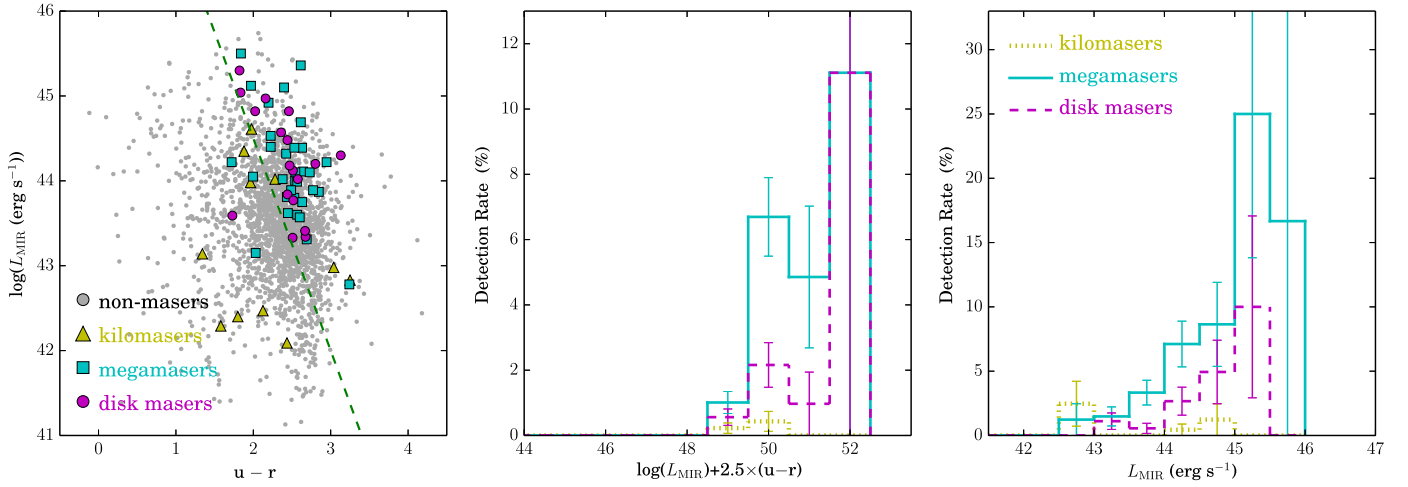


Figure 8. Left panel: the distribution of the MCP galaxies as a function of L_{MIR} and $u - r$; only the galaxies with available SDSS photometry are plotted here. The majority (88%) of the megamasers lie above the green dashed line corresponding to $\log(L_{\text{MIR}}) = -2.5 \times (u - r) + 49.5$. Middle panel: the maser detection rates as a function of $\log(L_{\text{MIR}}) = -2.5 \times (u - r) + 49.5$, for galaxies with $\log(L_{\text{MIR}}) > 43$, which includes all of the currently detected disks with SDSS photometry. Right panel: the maser detection rate as a function of L_{MIR} for sample galaxies having $\log(L_{\text{MIR}}) = -2.5 \times (u - r) + 49.5$.

conclusion from these trends is that the enhancement in the $f_{24\text{ }\mu\text{m}}/f_r$ ratios in megamasers reflects AGN activity, and thus the megamaser excitation is linked to this type of nuclear activity. If megamasers are more easily excited when the AGN strengths increase beyond a certain threshold, one would expect the total mid-IR luminosities of megamasers, which are correlated with the $f_{24\text{ }\mu\text{m}}/f_r$ ratios, to increase as the optical galaxy colors become bluer. We explore this possibility in Figure 8.

When the total mid-IR luminosities of the MCP galaxies are plotted as a function of their $u - r$ colors (Figure 8, left panel), it becomes apparent that the megamaser number densities increase for larger L_{MIR} and redder $u - r$ values. In fact, we find that most (90%) of the megamasers lie above the line defined by $\log(L_{\text{MIR}}) = -2.5 \times (u - r) + 49.5$. Note that greater values of $\log(L_{\text{MIR}}) + 2.5 \times (u - r)$ essentially mean a greater degree of enhancement of the $f_{24\text{ }\mu\text{m}}/f_r$ ratios by the AGN activity, and thus, once again, we are witnessing trends consistent with the idea that the AGN power may need to be above a certain high level to efficiently excite the megamasers.

Moreover, the consideration of the optical $u - r$ color in conjunction with L_{MIR} appears to open new ways to improve on the maser detection rates. When the maser detection rates are plotted as a function of $\log(L_{\text{MIR}}) + 2.5 \times (u - r)$ (Figure 8, middle panel), keeping only the galaxies with $\log(L_{\text{MIR}}) > 43$, which includes all of the detected disks with optical (SDSS) photometry, we find that greater values of $\log(L_{\text{MIR}}) + 2.5 \times (u - r)$ correspond to increasing enhancements in the megamaser and disk detection rates. In particular, for objects with $\log(L_{\text{MIR}}) + 2.5 \times (u - r) > 49.5$ (which lie above the dashed green line in Figure 8, left panel) and $\log(L_{\text{MIR}}) > 43$, the megamaser disk detection rates increase by at least a factor of 3 relative to those calculated for the entire sample of galaxies with available SDSS photometry, mounting from 0.7% to $\gtrsim 2\%$, for 94% completeness rates; for megamasers, the detection rate rises to 5.4%, for a completion rate of 88%. For brighter mid-IR sources, with $\log(L_{\text{MIR}}) > 44$, the detection rates of all megamasers and disks in particular increase to $\sim 8.3\%$ and 3.7% , respectively, with corresponding completion rates of 54% and 67%. These criteria manage to

minimize the exclusion of known disk megamasers while maximizing the inclusion of all types of megamasers.

3.3.5. Enhancing the Detection Rate by Including the g-band Absolute Magnitude

As seen in Section 3.1, 100% of the disk masers, out of 69% of all MCP galaxies with SDSS photometry, exhibit g-band absolute magnitudes $M_g < -19.7$, and thus, it has the potential to increase both the target sample and the megamaser completion fraction. Since M_g is independent of L_{MIR} and $u - r$, including this parameter in the analysis adds a new independent dimension to the study of the maser detection problem.

When plotting the $L_{\text{MIR}} + 2.5 \times (u - r)$ parameter as a function of M_g for all MCP galaxies with SDSS photometry (Figure 9), it is readily apparent here that the majority of the megamasers and disks lie in the top-right quadrant of the diagram. In fact, by choosing $\log(L_{\text{MIR}}) + 2.5 \times (u - r) \geq 49.5$ and $M_g < -19.7$ (marked in the figure by the dotted-dashed blue lines), we select a sample of galaxies that includes 95% of the disk megamasers and 79% of all known megamasers. The detection rates corresponding to these limits are $5.8\% \pm 0.9\%$ and $2.5\% \pm 0.6\%$ for the megamasers and disks, respectively, which is a welcome increase of >3 times relative to the current rates within the sample with SDSS photometric data (i.e., $1.9\% \pm 0.3\%$ for megamasers and $0.7\% \pm 0.2\%$ for disk masers).

Interestingly, this particular enhancement in the maser detection can be improved even more by choosing just slightly tighter cuts: for $\log(L_{\text{MIR}}) + 2.5 \times (u - r) \geq 49.8$ and $M_g < -20.2$ (marked in the figure by the dashed green lines), we include 68% of disk masers and 52% of the known megamasers, while their detection rates skyrocket to $7.8\% \pm 1.5\%$ and $3.7\% \pm 1.0\%$, respectively, which is an increase relative to the current rates by a factor of ~ 5 . Thus, these criteria offer the highest megamaser and disk detection rates for the highest degree of completeness, especially for the disk systems, among all of the criteria explored so far.

Moreover, if we select a sample based on the method described above, but only among the galaxies with

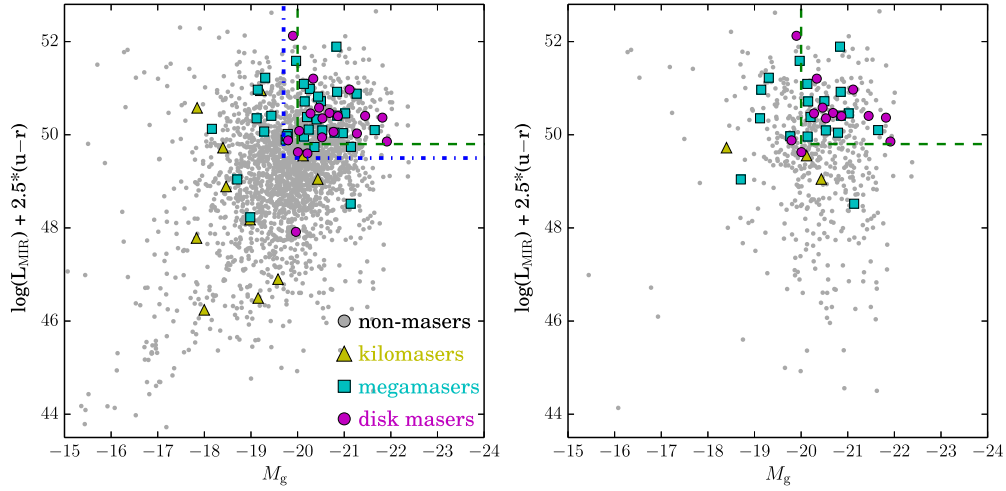


Figure 9. Left panel: the distribution of the sample galaxies in the M_g and $\log(L_{\text{MIR}}) + 2.5 \times (u - r)$ parameter space. The blue dashed lines correspond to $L_{\text{MIR}} + 2.5 \times (u - r) = 49.5$ and $M_g = -19.7$ while the green dashed lines indicate $L_{\text{MIR}} + 2.5 \times (u - r) = 49.8$ and $M_g = -20.2$. Right panel: same as the left panel, only for galaxies with $L_{\text{MIR}} \geq 10^{44} \text{ erg s}^{-1}$.

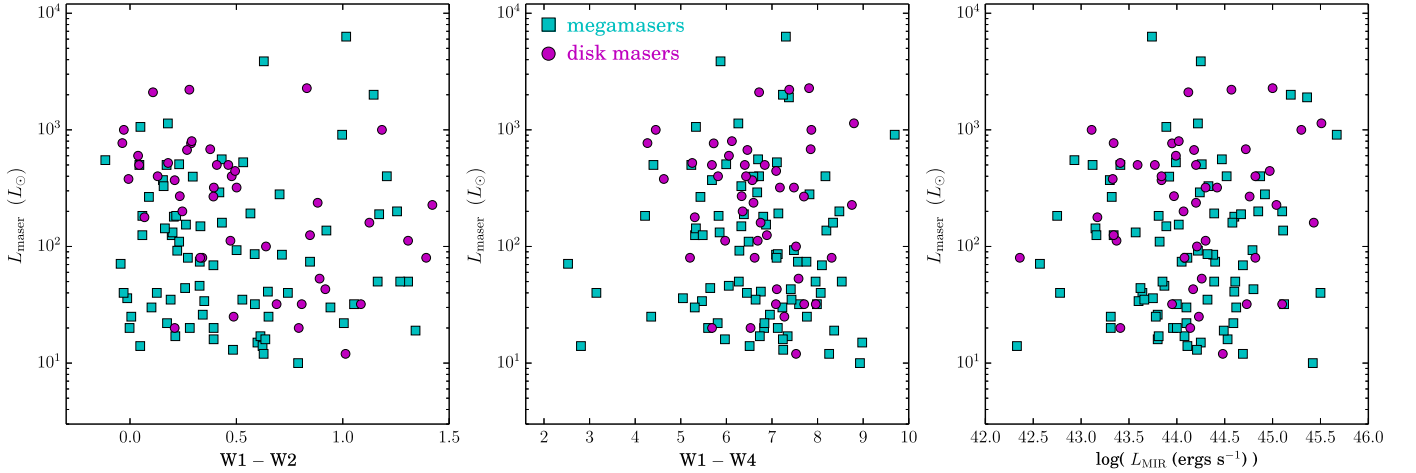


Figure 10. The isotropic maser luminosity $L_{\text{H}_2\text{O}}$ as a function of $W1 - W2$, $W1 - W4$, and $\log(L_{\text{MIR}})$. The filled cyan squares and the magenta circles represent megamasers and disk masers, respectively.

$L_{\text{MIR}} \geq 10^{44} \text{ erg s}^{-1}$, the detection rates increase further to $11.9\% \pm 2.5\%$ and $6.5\% \pm 2.1\%$ (corresponding to an increase of a factor of ~ 6 – 9 in the detection rates) for megamasers and disks, respectively, while the completeness rates reduce very little, to 44% for megamasers and 58% for the disks, which is still higher than when other criteria are employed (e.g., those targeting only *WISE* red objects, with a conservative $W1 - W2 > 0.5$ color cut, which recover only $< 30\%$ of known megamasers or disks; see Section 3.2.1).

3.4. The Dependence on the Isotropic Maser Luminosity

The utility of megamasers in either understanding the physics of SMBH accretion or in making accurate distance determinations, and thus for cosmological constraints, is most efficient when these systems are bright enough so that a high enough sensitivity is achieved with a relatively short observing time. It is therefore important to investigate the dependence of the total (isotropic) maser luminosities $L_{\text{H}_2\text{O}}$ on the AGN/galactic properties.

Figure 10 illustrates the relation between $L_{\text{H}_2\text{O}}$ and the *WISE* properties with the most potential association with strong maser emission, and thus with the highest megamaser detection rates,

as discussed in the previous sections: the $W1 - W2$ and $W1 - W4$ colors (the left and middle panels, respectively) and the integrated mid-IR luminosity (L_{MIR}). At first glance, there are no apparent relationships here. A closer look, however, reveals some interesting features.

A rather surprising trend is that the most luminous disk masers (i.e., those with $L_{\text{H}_2\text{O}} > 300 L_{\odot}$) appear to reside more preferentially in hosts with bluer *WISE* colors, i.e., with $W1 - W2 < 0.5$. This could suggest that brighter disk masers prefer the AGNs of bluer hosts, although this may simply be the result of the selection biases of the current maser samples: current maser surveys preferentially target optically known Seyferts (Constantin 2012) that are not optically obscured by high columns of obscuring dust, and thus, do not reprocess the central radiation at high enough levels to be seen as red in mid-IR. The fact that, among all megamasers, there is no particular correlation of $L_{\text{H}_2\text{O}}$ with $W1 - W4$ or L_{MIR} supports the targeting bias scenario and rejects a possible correlation between the water luminosity $L_{\text{H}_2\text{O}}$ and $W1 - W2$.

These trends do not necessarily contradict the previously suggested (albeit weak) dependence of the maser emission on the AGN strength by Zhu et al. (2011), Kondratko et al. (2006),

and Castangia et al. (2013), who employed the [O III] and X-ray luminosities as proxies for the AGN strength. While our findings of higher megamaser detection rates for redder $W1 - W4$ and stronger L_{MIR} suggest that enhanced AGN activity makes the detection of a water maser system easier, an association between these two types of activity cannot be described by a simple correlation between their strengths.

In addition to these mid-IR indicators of AGN activity, we also do not find any correlations between $L_{\text{H}_2\text{O}}$ and any other combinations of optical and mid-IR properties we have explored so far. This can be explained by recalling that megamasers often display significant variability and that the production rate of maser photons per unit volume depends on multiple physical parameters besides the strength of the AGN, e.g., the amplification path lengths, the warping angle of an accretion disk (particularly for the disk masers; Neufeld et al. 1994), the temperature difference between gas and dust in the masing environment (e.g., Gray et al. 2016), the degree of saturation, etc., which can vary substantially in different systems. We discuss in more detail these effects and their potential consequences on the correlations discussed so far in the next section.

4. Discussion: The Relationship between the AGN Strength and the Megamaser Detection Rate

This analysis provides new evidence for a strong relation between the megamaser detection rate R_{maser} and a variety of optical and mid-IR photometric galactic properties that can act as proxies for the presence and, likely, the strength of the incumbent AGN. Nevertheless, while we have uncovered ways of improving on the rate at which megamasers could be detected, from a current $<1\%$ to more than 15%, the trends we revealed here do not provide us with new or satisfactory improvements on our understanding of the physics of water maser excitation processes.

The correlations found to date between the detection rate as well as the strength and the morphology of the water maser emission and the nuclear properties of their host have been explored under the rather simple assumption that the megamaser emission originates primarily from the thin accretion disk that is obliquely illuminated by a central X-ray source (e.g., Neufeld & Maloney 1995, Neufeld 2000). In this scenario, the total maser luminosity $L_{\text{H}_2\text{O}} \propto L_{\text{AGN}}$ (where L_{AGN} is the bolometric luminosity of the AGN), and thus a correlation between R_{maser} and L_{AGN} becomes reasonable because a higher L_{AGN} leads to a higher $L_{\text{H}_2\text{O}}$, making megamasers easier to detect.

Indeed, we found that when compared to non-masers and kilomasers, megamasers do appear to favor more luminous hosts as well as stronger optical and mid-IR emitters. However, among megamasers alone, there is no clear (or at most tentative) relation between the strength of the water maser emission and that of the AGN activity, whether this is measured via optical photometry (M_g), optical line emission (e.g., $L_{[\text{O III}]}$; Zhu et al. 2011; Constantin 2012), X-ray activity (e.g., Kondratko et al. 2006; Castangia et al. 2013), or its reprocessed counterpart in the mid-IR by the surrounding dust (L_{MIR} or $W1 - W4$; this study).

Particularly puzzling in this regard is the low-luminosity nature of the AGN in NGC 4258. In this prototypical megamaser disk galaxy, the accretion rate of the SMBH is estimated to be $10^{-4} M_{\odot} \text{yr}^{-1}$ and the Eddington ratio is

$\sim 1 \times 10^{-4}$ (Herrnstein et al. 2005), showing that strong megamasers such as this one do not necessarily require high Eddington ratios. Therefore, it is not clear why R_{maser} diminishes significantly when the associated AGN becomes weaker. Evidence for variability in both the AGN activity on multiple timescales (e.g., Ulrich et al. 1997) and that of the associated maser emission (e.g., Pesce et al. 2015) suggests that such variations, especially when they are not measured simultaneously in other wavelengths, may easily smear out a correlation between the AGN and megamaser strengths.

It is pretty clear that more subtle physics must be involved, and we explore here two possible improvements in our understanding of these phenomena: (1) the potential for megamasers to arise from or with AGN outflows, and (2) the likelihood that megamasers originate from nearly edge-on subparsec warped gas disks.

4.1. Connecting Megamasers with AGN Outflows

AGN-driven gas outflows are generally good tracers of AGN activity in general, and of AGN feedback in action in particular (e.g., Rupke et al. 2005; Greene et al. 2012). Powerful outflows are found to significantly influence the surrounding interstellar matter, and in particular, AGN outflows appear easily able to shock the circumnuclear gases leading to densities and temperatures that are suitably high for generating water maser emission. For the efficient excitation of 22 GHz water masers, the required number density and temperature of the molecular gas are 10^8 – 10^{10}cm^{-3} and 400–1000 K, respectively (Herrnstein et al. 2005; Gray et al. 2016).

Maybe not unexpected is the fact that both the outflow rate of molecular gas and the power of AGN outflows are found to depend strongly on L_{AGN} (e.g., Fiore et al. 2017). In the case of ionized gas, the kinematic signature of AGN outflows is very common in luminous type 2 AGNs, showing a clear increasing trend of the outflow fraction from 20% to almost 100% as the [O III] luminosity increases from $10^{39} \text{erg s}^{-1}$ to $10^{42} \text{erg s}^{-1}$ (Woo et al. 2016; see also Kang et al. 2017 for $\text{H}\alpha$ line-based AGN fractions). Thus, it is natural to speculate that as the AGN emission becomes stronger and the probability of finding powerful AGN outflow gets higher, the circumnuclear gas is more likely to get shocked and produce maser activity, leading to the observed correlation between R_{maser} and AGN strength.

While this simple picture is appealing, it remains practically unexplored. Currently, high-resolution VLBI imaging of masers in jet systems only exists in a few galaxies, e.g., NGC 1052 (Claussen et al. 1998), Circinus (Greenhill et al. 2003), NGC 1068 (Gallimore et al. 2001), and Mrk 348 (Peck et al. 2003), and thus, there are not enough statistical data to probe the above-mentioned correlations.

4.2. The Role of Maser Disk Warping

That at least a fraction of megamasers originate in a disk-like configuration is now well established. The real fraction of disk megamasers could easily be larger than what is currently observed as their detection requires that the gas disk be nearly edge-on (i.e., within a few degrees from being edge-on; Kuo et al. 2011, 2013; Reid et al. 2013; Gao et al. 2016). The nearly edge-on disk is necessary in order to provide the longest amplification path length that can lead to the strongest maser amplification. Previous maser surveys primarily targeted Seyfert 2 galaxies mainly because of the higher likelihood of

finding nearly edge-on disks in these systems, under the assumption that the standard model of AGNs (Antonucci 1993) holds true. While the disk inclination is very likely the primary reason for the low maser disk detection rates, this parameter does not offer much interpretation for the correlation between R_{maser} and the strength of the AGN, because it is mainly a geometrical effect.

To explain the dependence of R_{maser} on L_{AGN} for disk masers, one has to first understand how the necessary conditions for water maser excitation may depend on the geometry itself. Based on the standard theory of a thin steady-state accretion disk, the number density in the midplane of the disk can be written as a function of the radial distance r as (Neufeld & Maloney 1995; Herrnstein et al. 2005)

$$n_{\text{H}_2} = \frac{GM_0\dot{M}}{3\pi(2\pi)^{1/2}\alpha r^3 c_s^3 m_{\text{H}_2}}, \quad (1)$$

where M_0 is the central mass, \dot{M} is the accretion rate, α is the Shakura–Sunyaev parameter of the kinematic viscosity (Shakura & Sunyaev 1973), c_s is the speed of sound, and m_{H_2} is the mass of the hydrogen molecule. By assuming $L_{\text{AGN}} = 0.1\dot{M}c^2$, where c is the speed of light, $\alpha = 0.1$, and $c_s = 2.3 \text{ km s}^{-1}$ (corresponding to the gas temperature of 800 K), we can re-express n_{H_2} as a function of the Eddington ratio η_{Edd} and M_0 as

$$n_{\text{H}_2} = 7.8 \times 10^8 \left(\frac{M_0}{10^7 M_\odot} \right) \left(\frac{\eta_{\text{Edd}}}{10^{-4}} \right) \left(\frac{r}{0.1 \text{ pc}} \right)^{-3} \text{ cm}^{-3}. \quad (2)$$

From here, it is clear that as long as the gas can be heated to a few hundred Kelvin, the density requirement for maser excitation can be easily fulfilled at highly sub-Eddington systems, such as NGC 4258, at subparsec scales. By comparison with the needed gas density for maser excitation, what is actually more difficult to fulfill is the temperature requirement. We also note, however, that, for NGC 4258, the assumption of steady-state accretion might not hold (Gammie et al. 1999).

In the standard picture of maser excitation in an accretion disk (Neufeld et al. 1994; Neufeld & Maloney 1995), which is established based on the study of NGC 4258, the gas disk has to be warped so that the high-density midplane gas can be directly illuminated by the central X-ray source to raise the gas temperature T_{gas} above 400 K. In a completely flat disk, the midplane is shielded from the heating source and the gas remains too cold (i.e., $T_{\text{gas}} < 100 \text{ K}$) to lase; viscous heating alone is insufficient to heat the disk to a sufficient temperature. Therefore, an external source of torque is needed in order to warp the disk so that the gas receives the sufficient X-ray heating necessary to excite the maser. In other words, the weaker the AGN is, the greater the degree of warping needs to be in order for the gas to receive sufficient heating flux F_X .

Disk warping plays yet another important role in producing or enhancing the maser emission. After T_{gas} rises above 400 K, the volume rate of maser photon production depends significantly on the temperature difference between gas and dust (Gray et al. 2016), which in turn depends primarily on F_X (Neufeld et al. 1994). While these dependences are highly nonlinear, mainly due to their dependence on other physical parameters, such as pressure and gas density in the disk, there is tentative evidence for a correlation between the X-ray flux

and the increase in the maser emissivity (Neufeld et al. 1994; Neufeld 2000); these calculations show that the amount of heating flux received by the gas in the disk increases with the obliquity of the disk (i.e., the tilt or the warping of the disk), and thus it is likely to result in higher maser emissivity. A major caveat here is that the maser emissivity also depends on the bolometric luminosity of the central AGN: while an increase in the X-ray luminosity can lead to an increase in maser emissivity, an increase in the bolometric luminosity that is not necessarily driven by an increase in X-ray luminosity will decrease the maser emissivity because the temperature difference between gas and dust becomes smaller. Hence, the exact type of AGN activity will play a crucial role in determining the type of the emergent maser emission, and the exact interdependence remains a conundrum.

4.3. The Probability of Finding Disks with Different Degrees of Warping

Warping a gas disk within the gravitational sphere of influence (R_{inf}) of the central SMBH is difficult. There are only two mechanisms that have been demonstrated to be able to warp the subparsec maser disks effectively. One way is via the Bardeen–Peterson effect (e.g., Caproni et al. 2007), which is caused by the interaction between the BH spin and the gas disk; however, this mechanism can only warp the disk in NGC 4258 by $\sim 3^\circ$ – 4° on a timescale of a few $\times 10^8 \text{ yr}$ (Bregman & Alexander 2012), whereas the maser disk in this galaxy displays a warp angle of $\sim 8^\circ$ (Herrnstein et al. 2005). A potentially much more efficient warping mechanism is resonant relaxation (Bregman & Alexander 2009; Bregman & Alexander 2012), in which the gas disk is warped due to the residual torque produced by stars residing within R_{inf} . In this situation, the maser disk can be warped on a smaller timescale of $\sim 10^7 \text{ yr}$; however, the probability of producing warping angles of $\sim 10^\circ$ is considerably smaller than that of producing warping angles of just a few degrees.

While the validity of the proposed warping mechanisms still needs to be constrained observationally, it is quite reasonable to conjecture that the probability of finding disks with smaller warping angles could be higher than that of finding disks with larger warping angles. As a consequence, the maser detection rates R_{maser} will be expected to correlate with the AGN strength because as L_{AGN} increases, the required degree of the warping angles that would satisfy the masing conditions gets smaller, and hence, the probability of finding these disks becomes higher.

We also note here that for luminous AGNs where the Eddington ratio η_{Edd} gets above 0.1, another heating mechanism comes into play, and the requirement of disk warping for maser excitation can become less stringent. As demonstrated by the results of the axisymmetric radiation hydrodynamic simulations of Namekata & Umemura (2016), the midplane temperature of a completely flat dusty gas disk without warping around a BH of mass $10^7 M_\odot$ (i.e., the typical BH mass measured for maser disks) with $\eta_{\text{Edd}} = 0.77$ can rise above 400 K at the radius of 0.5 pc. In this case, the heat transfer through collision between the gas in the midplane and the gas above/below the midplane, which can be directly heated by X-rays, may become efficient enough so that the midplane gas can be warmed significantly without the disk being warped and illuminated directly. Thus, it is possible that the maser detection rate R_{maser} increases considerably for high L_{AGN}

Table 2
Warping Angles of Five Disk-maser Systems

Galaxy Name	Distance (Mpc)	L_{AGN} (erg s ⁻¹)	η_{Edd}	dp/dr (degree mas ⁻¹)	θ_{warp} (degree)	Reference
NGC 4258	7.6	1.0×10^{42}	2×10^{-4}	5.2 ± 0.3	9.3 ± 1.7	Humphreys et al. (2013)
NGC 6323	104.6	2.4×10^{43}	0.018	13.2 ± 2.6	3.1 ± 0.6	Kuo et al. (2015)
UGC 3789	47.7	2.5×10^{44}	0.13	-2.0 ± 1.1	1.0 ± 0.6	Reid et al. (2013)
NGC 5765b	120.7	3.3×10^{44}	0.02	-3.5 ± 0.4	0.7 ± 0.1	Gao et al. (2016)
NGC 6264	139.7	5.6×10^{44}	0.132	18.3 ± 1.8	3.2 ± 0.3	Kuo et al. (2013)

Note. Column 1: name of the galaxy. Column 2: the distance to the galaxy used for converting the angular scale to the physical scale. Column 3: the bolometric luminosity of the AGN. With the exception of NGC 5765b, the bolometric luminosities are from Greene et al. (2010). For NGC 5765b, the bolometric luminosity is estimated from the [O III] luminosity reported in Gao et al. (2017), with the bolometric correction from Liu et al. (2009). Column 4: the Eddington ratios. Column 5: the change of the position angle with the angular radius. These are the best-fit warp parameters from the three-dimensional Bayesian modeling of the observed maser disks, with the corresponding references listed in Column 7. Column 6: the warping parameter of the maser disk, θ_{warp} , which is evaluated from $\theta_{\text{warp}} = dp/dr(r_{\text{in}} - r_{\text{out}}) + d^2p/dr^2(r_{\text{in}}^2 - r_{\text{out}}^2)$, where r_{in} and r_{out} are 0.17 and 0.37 pc, respectively. $d^2p/dr^2 = -0.24 \pm 0.02$ for NGC 4258, and it is unavailable for the other galaxies except for UGC 3789, where it is set to zero given that the warp is extremely small. Column 7: the references from which we obtained the best-fit warp parameters.

due solely to the fact that the temperature requirement for maser excitation becomes increasingly easier to fulfill.

To find evidence for these ideas, we compare the degree of warping θ_{warp} (or how much the disk is bent) of the five disk-maser systems (NGC 6323, NGC 6264, NGC 5765b, UGC 3789, and NGC 4258) that are found, to date, to have well-defined disk structures in high-sensitivity VLBI observations. All of these systems have been modeled in three dimensions, and the warping parameters are constrained with high accuracy (i.e., the position angles of the maser disk at different radii can be constrained to better than 2° for systems such as NGC 4258). We summarize the warping parameters and other basic parameters for each of these five galaxies in Table 2, where we sort them in increasing order of their L_{AGN} . Note that we do not include disk-maser systems such as Circinus (Greenhill et al. 2003) in this analysis because these systems do not have acceleration measurements for their maser features, which are required to constrain maser positions along the line of sight in accurate three-dimensional modelings of disk masers (Reid et al. 2013).

The degree of disk warping, θ_{warp} , is generally defined as the change in the position angle of the disk from the inner radius r_{in} to the outer radius r_{out} of the disk. We note, however, that different maser disks usually exhibit different r_{in} and r_{out} , which makes any comparison of the warping quite challenging. For the sake of consistency, we redefine θ_{warp} as the change in the position angle of the disk over a radial extent of 0.2 pc, stretching from $r_{\text{in}} = 0.17$ pc to $r_{\text{out}} = 0.37$ pc; $r_{\text{in}} = 0.17$ pc is the inner radius of the maser disk in NGC 4258 (Herrnstein et al. 2005).

Among these five galaxies, NGC 4258 has the lowest bolometric luminosity and Eddington ratio ($L_{\text{AGN}} = 10^{42}$ erg s⁻¹; $\eta_{\text{Edd}} = 2 \times 10^{-4}$), and the largest $\theta_{\text{warp}} = 9.3 \pm 1.7$ (Humphreys et al. 2013). As L_{AGN} increases by two orders of magnitude, θ_{warp} becomes significantly smaller, by at least a factor of 3 and reaching even an order of magnitude. Unfortunately, the Eddington ratios of the four more luminous maser disks are similar and thus are not particularly helpful in identifying additional trends with the degree of warping.

From these comparisons, one can easily see that as the AGN strength increases, θ_{warp} drops and can become quite negligible at the highest AGN luminosities among our sample. In light of a possible strong link between the AGN and the water masing

strengths, this would translate into less warped maser disks found with maser searches targeting objects with higher Eddington ratios. While the number statistics are currently too small to confirm any clear relation between the maser disk warping and the AGN strength, as well as to provide sensible constraints of the detection rates of maser disks with a certain degree of warping, the general trend is well consistent with the proposed picture. If and when more high-quality images of disk-maser systems become available, we will be in a better position to test and quantify this proposed relationship between the warping angles of the disk masers and the AGN strength and accretion efficiency, and thus should provide crucial insights into the link between megamaser excitation and SMBH accretion disks.

5. Conclusions: Guidance for Future Maser Surveys

To reach the ultimate potential of H₂O megamasers for measuring a percent-level H_0 , as well as for a significant increase in the number of accurately measured masses of SMBHs, we need efficient searches for new megamaser disk systems. We address here ways in which we could greatly improve our quest for finding these exotic systems by exploring the maser host galaxy characteristics that relate to, and thus possibly nurture the production of, powerful masers in their centers.

Using data from the *Wide-Field Infrared Survey Explorer* (WISE), with optical photometry from SDSS as auxiliary information, we present here a thorough analysis of the photometric properties of the largest sample of galaxies surveyed for H₂O maser emission in 22 GHz, with the goal of better constraining the previously proposed connection between water masing activity and the circumnuclear dust absorption and radiation reprocessing in galaxy centers. To date, this kind of information is scarce, as no systematic study of the multiwavelength properties of the galaxies observed in H₂O maser emission at 22 GHz has been performed for a sound statistical sample. We only now have the statistics to pursue such an investigation.

Our main results are summarized in Table 3 and are briefly discussed as follows:

1. **Red W1 – W2 colors.** The mid-IR color cuts for selecting red/dusty AGNs reveal a dramatic increase in the maser detection rates (up to $\sim 10\%$ for all masers, and

Table 3
Effective Search Criteria for Megamasers and Disks

Search Criteria	% All MCP Galaxies	R_{maser} %	C_{maser} %	R_{Mmaser} %	C_{Mmaser} %	R_{disk} %	C_{disk} %	$R_{\text{disk}}^{100-300}(N_{\text{disk}})^a$
<i>WISE</i> ($S/N > 3$)	86	3.3 ± 0.3	100	2.7 ± 0.2	98	0.9 ± 0.1	100	...
SDSS photometry	57	2.3 ± 0.3	40	1.9 ± 0.3	40	0.7 ± 0.2	40	0.7% (163)
$W1 - W2 > 0.5$	18	8.8 ± 1.1	45	7.0 ± 1.0	44	2.3 ± 0.5	39	0.9% (3)
$W1 - W2 > 0.8$	9	9.5 ± 1.6	25	8.0 ± 1.4	26	3.3 ± 0.9	30	1.8% (1)
$W1 - W2 > 0.5$ $W1 - W4 > 7$	6	18.2 ± 2.5	32	14.9 ± 2.3	32	4.7 ± 1.3	28	2.8% (3)
$W1 - W2 > 0.4$ $W1 - W4 > 6$	17	10.5 ± 1.2	48	8.5 ± 1.1	48	3.1 ± 0.6	49	1.4% (5)
$L_{\text{MIR}} > 10^{44} \text{ erg s}^{-1}$	27	7.4 ± 0.8	53	6.7 ± 0.8	58	2.5 ± 0.5	62	1.6% (36)
$L_{\text{MIR}} > 10^{43} \text{ erg s}^{-1}$	76	4.4 ± 0.4	90	3.8 ± 0.3	96	1.4 ± 0.2	98	0.9% (170)
$\log(L_{\text{MIR}}) + 2.5(u - r) > 49.5$ $L_{\text{MIR}} > 10^{43} \text{ erg s}^{-1}$	44	4.8 ± 0.7	79	4.4 ± 0.7	90	1.7 ± 0.2	94	1.5% (67)
$\log(L_{\text{MIR}}) + 2.5(u - r) > 49.8$ $M_g < -20.2$	14	7.8 ± 1.5	43	7.8 ± 1.5	52	3.7 ± 1.0	68	3.3% (81)
$\log(L_{\text{MIR}}) + 2.5(u - r) > 49.8$ $M_g < -20.2$ $L_{\text{MIR}} > 10^{44} \text{ erg s}^{-1}$	6	11.8 ± 2.8	29	11.8 ± 2.8	44	6.5 ± 2.1	58	5.6% (20)

Notes. R_{maser} , R_{Mmaser} , and R_{disk} are the detection rates of all masers, megamasers, and disks, respectively. C is the completeness rate, listed separately for all masers, megamasers, and disks. The highest detection and completion rates for megamasers and disks are highlighted in bold. Note that the detection rates and completeness rates shown in the last three rows of this table are calculated relative to the entire sample of galaxies with available SDSS photometry.

^a N_{disk} = predicted number of new disk masers that could be detected based on each criteria, from the SDSS DR14 sample of nearby galaxies with photo- $z < 0.1$, photo- $z_{\text{Err}} < 0.01$, photo- $z_{\text{Err}}/\text{photo-}z < 1/3$, and distance between 100 and 300 Mpc (a total of 23,277 galaxies). $R_{\text{disk}}^{100-300}$ = the disk detection rate prorated for this particular distance range.

$\sim 7\%$ for megamasers and disks, depending on the exact criteria involved in defining the red *WISE* galaxies, which is a boost by at least a factor of 4 relative to the current rates). Nevertheless, these criteria, which link once again the masing activity with dusty/obscured black hole accretion, correspond to a rather small maser completeness rate: they would miss the bulk of the megamaser disks out there, as the majority ($\sim 60\%$) of the masers and disks are found to be hosted by *WISE* blue galaxies. Also, the potential pool of such galaxies remains small, as only 16% of our entire sample satisfy this criterion.

- Red $W1 - W2$ and $W1 - W4$ colors. By adding the $W1 - W4$ information, we are able to avoid galaxies with low emission in $W4$ at $22 \mu\text{m}$ where the maser detection rates are the lowest and to raise the detection rates of all masers and megamasers to $\sim 18\%$ and $\sim 15\%$, respectively, depending on how stringently red are the considered galaxies. The completeness rate can be higher than 48% for detection rates that are three times better than the current ones. While with the most stringent red colors the detection rates can be the highest among all other sample selection methods we have explored here, they would be able to target only 30% of the megamasers, meaning that we would still miss the bulk of the maser disks. Because there are only $\sim 6\%$ of galaxies that comply with these criteria, these surveys are less prohibitive in terms of the total observing time.
- $L_{\text{MIR}} > 10^{44} \text{ erg s}^{-1}$: By selecting galaxies with luminous mid-IR emission, the maser detection rates can

be increased by a factor of 2–3 from the current ones. While the maser detection rates are lower in comparison with the two previous methods, they are still a factor of at least 3 larger than the current ones, with a rate of completeness that reaches $\sim 60\%$ for megamasers and disks. For a slightly lower mid-IR luminosity, i.e., $L_{\text{MIR}} > 10^{43} \text{ erg s}^{-1}$, the pool of available galaxies to be surveyed increases by a factor of 3, and the disk completion rates rise to $\sim 100\%$ for megamaser and disk detection rates that almost double the current detections.

- $\log(L_{\text{MIR}}) + 2.5 \times (u - r) > 49.5$ and $L_{\text{MIR}} > 10^{43} \text{ erg s}^{-1}$. A combination of intrinsically bright mid-IR emission and optical colors results in reasonably high detection rates (double the current ones) with only a small likelihood of not surveying disks or megamasers in general (the completion rates are $> 90\%$). These criteria are particularly useful in avoiding kilomasers, targeting most efficiently the megamaser activity, with or without an obvious disk.
- $\log(L_{\text{MIR}}) + 2.5 \times (u - r) > 49.8$ and $M_g < -20.2$. By combining the total mid-IR luminosity with optical colors and optical brightness, the maser detection rates rise to $\sim 8\%$ and $\sim 4\%$ for the megamasers and disks, respectively; this represents an enhancement of a factor of 4–5 times relative to the current ones, among all surveyed galaxies with SDSS photometry. While the detection rate of megamasers is comparable to those drawn from samples of galaxies with $W1 - W2 > 0.8$, the completeness is increased threefold, especially for the disk

masers: 52% of megamasers and 68% of disk masers satisfy these criteria. The total number of galaxies in this parameter range is also two times larger than that in the case of the $W1 - W2 > 0.8$ limit, thus increasing the total number of potential disk detections.

6. $\log(L_{\text{MIR}}) + 2.5 \times (u - r) > 49.8$ and $M_g < -20.2$ plus $L_{\text{MIR}} > 10^{44} \text{ erg s}^{-1}$. When an additional condition on the integrated mid-IR brightness is employed, the megamaser and disk detection rates increase to $\sim 12\%$ and $\sim 6\%$, respectively (a factor of 6–9 increase relative to the current rates), while the completeness remains relatively high (i.e., above 44% or higher). These criteria should constitute the most efficient way of hunting for the next megamaser disks.

Of course, one of the most pressing questions is finding how many unsurveyed galaxies are in these particular parameter spaces, and how many megamasers they might detect. What really matters for improving H_0 or SMBH statistics is not so much the completeness as the sheer numbers. While previous maser surveys might have somewhat exhausted the main samples of nearby spectroscopically identified galaxies, there is a significantly higher number of galaxies with photometric redshifts that have not yet been explored for water maser emission.

Working with, for example, the SDSS DR14 sample of nearby galaxies with photometric redshifts, a best match to the redshift (or distance) distribution of the MCP samples discussed here is given by the selection of all galaxies with $\text{photo-}z < 0.1$, $\text{photo-}z_{\text{Err}} < 0.01$, $\text{photo-}z_{\text{Err}}/\text{photo-}z < 1/3$, and distance between 100 and 300 Mpc (for objects closer than 100 Mpc, the photometric redshifts are not reliable).

Tailoring our analysis for this particular distance range (which results in slightly smaller detection rates for maser galaxies of all types) and applying the photometric criteria summarized above, we find that quite a high number of megamaser disk systems are still to be detected. These number predictions are listed in the last column of Table 3, which reflects the potential to find 20 (or 81) new maser disks from a survey of carefully chosen ~ 360 (or ~ 2500) galaxies that obey the last (or the second to last) set of criteria listed in Table 3, making these results supremely valuable. We caution, however, that this success rate may be subject to a preselection on strong narrow-line emission activity, as it was generally employed in building the MCP samples.

Regarding the need and use of the new detections of megamaser disks, a 1% accuracy in H_0 can potentially be achieved via either (i) the measurement of $\sim 10\%$ accuracy distances to $\gtrsim 100$ disk-maser systems or (ii) the measurement of high-accuracy (3%) distances to ~ 10 disk-maser galaxies (e.g., Greenhill et al. 2009). The number of disk masers from which one can obtain distances with $\sim 10\%$ accuracy is likely to remain below 100 in the following decade, even when applying our most efficient predictions for selection (Table 3), as the survey time would become prohibitively long, making the first option utterly impractical. While the current VLBI sensitivity can provide the needed 3% accuracy only for one maser disk (NGC 4258), the Next Generation Very Large Array (ngVLA) within the VLBI is bound to make that accuracy possible for a larger number of maser disks, making the second option for achieving 1% H_0 actually feasible: the current maser surveys provide a fraction of $\sim 1/7$ disk masers with sufficient quality for 3% accuracy in the distance

measurements, suggesting that all we need is the discovery of ~ 70 new maser disks; with the $\sim 6\%$ detection rate we predict here, we will need to survey ~ 1200 narrow emission-line galaxies that satisfy the criterion, and this is doable with a GBT scanning time of ~ 10 minutes per galaxy, or a total of 200 GBT hours (which is the typical GBT time awarded to the MCP per year before 2013).






The work presented here constitutes our first step toward enhancing the maser detection rate. We find that although employing mid-IR criteria considerably improves the megamaser detection rates, the mid-IR emission alone does not seem to be particularly sensitive or constraining to the maser pumping mechanism. On the other hand, the maser disk detection could remain the only way to acknowledge accreting SMBHs in *WISE* blue hosts whose nuclei do not show clear signs of AGN-like optical nebular properties, and thus could provide an improved way to compute a refined census of active black holes in galaxy centers. A better understanding of the individual contributions from the host starlight, the nuclear star formation, as well as the central AGN to the mid-IR properties, and thus to the effects of each of these activities on the water masing processes, can be achieved with SED fittings of the light emitted by the hosts of the various subtypes of masers and non-masers. We will be presenting this analysis in a future paper (C.-Y. Kuo et al. 2019, in preparation).

We gratefully acknowledge the anonymous referee for a very thorough and insightful review that improved this manuscript. This publication is supported by the Ministry of Science and Technology, R.O.C. under the project 104-2112-M-110-014-MY3. A.C. acknowledges support from 4-VA, a collaborative partnership for advancing the Commonwealth of Virginia, along with the hospitality of the The National Radio Astronomical Observatory's North American ALMA Science Center in Charlottesville, VA, where part of this work was done. J.-H.W. acknowledges support by the Basic Science Research Program through the National Research Foundation of Korea (No. 2017R1A5A1070354).

This work has made use of data products from the *WISE* and the SDSS. *WISE* is a joint project of the University of California, Los Angeles, and the Jet Propulsion Laboratory/California Institute of Technology, funded by the National Aeronautics and Space Administration. SDSS is managed by the Astrophysical Research Consortium for the Participating Institutions of the SDSS-III Collaboration including the University of Arizona, the Brazilian Participation Group, Brookhaven National Laboratory, Carnegie Mellon University, University of Florida, the French Participation Group, the German Participation Group, Harvard University, the Instituto de Astrofísica de Canarias, the Michigan State/Notre Dame/JINA Participation Group, Johns Hopkins University, Lawrence Berkeley National Laboratory, Max Planck Institute for Astrophysics, Max Planck Institute for Extraterrestrial Physics, New Mexico State University, New York University, Ohio State University, Pennsylvania State University, University of Portsmouth, Princeton University, the Spanish Participation Group, University of Tokyo, University of Utah, Vanderbilt University, University of Virginia, University of Washington, and Yale University. This research has made use of the NASA/IPAC Extragalactic Database (NED), which is operated by the Jet Propulsion Laboratory, California Institute of Technology, under contract with the National Aeronautics and Space Administration. Funding for SDSS has been provided by

the Alfred P. Sloan Foundation, the Participating Institutions, the National Science Foundation, and the U.S. Department of Energy Office of Science. The SDSS Web site is <http://www.sdss.org/>.

ORCID iDs

C. Y. Kuo  <https://orcid.org/0000-0001-6211-5581>
 A. Constantin  <https://orcid.org/0000-0002-2441-1619>
 D. Pesce  <https://orcid.org/0000-0002-5278-9221>
 Lei Hao  <https://orcid.org/0000-0003-2478-9723>
 Ingyin Zaw  <https://orcid.org/0000-0002-1083-598X>

References

- Abazajian, K. N., Adelman-McCarthy, J. K., Agüeros, M. A., et al. 2009, *ApJS*, **182**, 543
- Ahn, C. P., Alexandroff, R., Allende, P., et al. 2014, *ApJS*, **211**, 17
- Aird, J., Coil, A. L., & Georgakakis, A. 2017, *MNRAS*, **465**, 3390
- Alonso-Herrero, A., Pérez-González, P. G., Alexander, D. M., et al. 2006, *ApJ*, **640**, 167
- Antonucci, R. 1993, *ARA&A*, **31**, 473
- Antonucci, R. R. J., & Miller, J. S. 1985, *ApJ*, **297**, 621
- Assef, R. J., Stern, D., Kochanek, C. S., et al. 2013, *ApJ*, **772**, 26
- Baldwin, J. A., Phillips, M. M., & Terlevich, R. 1981, *PASP*, **93**, 5
- Barth, A. J., Sarzi, M., Rix, H.-W., et al. 2001, *ApJ*, **555**, 685
- Batchelor, R. A., Jauncey, D. L., & Whiteoak, J. B. 1982, *MNRAS*, **200**, 19
- Bonvin, V., Courbin, F., Suyu, S. H., et al. 2017, *MNRAS*, **465**, 4914
- Braatz, J. A., & Gugliucci, N. E. 2008, *ApJ*, **678**, 96
- Braatz, J. A., Henkel, C., Greenhill, L. J., Moran, J. M., & Wilson, A. S. 2004, *ApJ*, **617**, 29
- Braatz, J. A., Reid, M. J., Humphreys, E. M. L., et al. 2010, *ApJ*, **718**, 657
- Braatz, J. A., Wilson, A. S., & Henkel, C. 1996, *ApJS*, **106**, 51
- Braatz, J. A., Wilson, A. S., & Henkel, C. 1997, *ApJS*, **110**, 321
- Bregman, M., & Alexander, T. 2009, *ApJ*, **700**, 192
- Bregman, M., & Alexander, T. 2012, *ApJ*, **748**, 63
- Caproni, A., Abraham, Z., Livio, M., & Mosquera Cuesta, H. J. 2007, *MNRAS*, **379**, 135
- Castangia, P., Panessa, F., Henkel, C., Kadler, M., & Tarchi, A. 2013, *MNRAS*, **436**, 3388
- Cen, R. 2012, *ApJ*, **755**, 28
- Claussen, M. J., Diamond, P. J., Braatz, J. A., Wilson, A. S., & Henkel, C. 1998, *ApJ*, **500**, 129
- Claussen, M. J., & Lo, K.-Y. 1986, *ApJ*, **308**, 592
- Constantin, A. 2012, *JPhCS*, **372**, 012047
- Constantin, A., Green, P., Aldcroft, T., et al. 2009, *ApJ*, **705**, 1336
- Constantin, A., Hoyle, F., & Vogeley, M. S. 2008, *ApJ*, **673**, 715
- Constantin, A., Shields, J. C., Ho, L. C., et al. 2015, *ApJ*, **814**, 149
- Crenshaw, D. M., Kraemer, S. B., Hutchings, J. B., et al. 2000, *AJ*, **120**, 1731
- Crenshaw, D. M., Kraemer, S. B., Schmitt, H. R., et al. 2010, *AJ*, **139**, 871
- Das, V., Crenshaw, D. M., Kraemer, S. B., & Deo, R. P. 2006, *AJ*, **132**, 620
- Diamond-Stanic, A. M., Fan, X., & Brandt, W. N. 2009, *ApJ*, **699**, 782
- Donley, J. L., Rieke, G. H., Pérez-González, P. G., Rigby, J. R., & Alonso-Herrero, A. 2007, *ApJ*, **660**, 167
- Ferrarese, L., & Merritt, D. 2000, *ApJ*, **539**, 9
- Fiore, F., Feruglio, C., & Shankar, F. 2017, *A&A*, **601**, A143
- Fiore, F., Grazian, A., Santini, P., et al. 2008, *ApJ*, **672**, 94
- Fischer, T. C., Crenshaw, D. M., Kraemer, S. B., Schmitt, H. R., & Tripp, M. L. 2010, *AJ*, **140**, 577
- Gao, F., Braatz, J. A., Reid, M. J., et al. 2016, *ApJ*, **817**, 128
- Gao, F., Braatz, J. A., Reid, M. J., et al. 2017, *ApJ*, **834**, 52
- Gallimore, J. F., Henkel, C., Baum, S. A., et al. 2001, *ApJ*, **556**, 694
- Gammie, C. F., Narayan, R., & Blandford, R. 1999, *ApJ*, **516**, 177
- Gebhardt, K., Bender, R., & Bower, G. 2000, *ApJ*, **539**, 13
- Gebhardt, K., & Thomas, J. 2009, *ApJ*, **700**, 1690
- Georgakakis, A., Aird, J., Schulze, A., et al. 2017, *MNRAS*, **471**, 1976
- Georgantopoulos, I., Georgakakis, A., Rowan-Robinson, M., & Rovilos, E. 2008, *A&A*, **484**, 671
- Graham, A. W., Onken, C., Athanassoula, E., & Combes, F. 2011, *MNRAS*, **412**, 2211
- Gray, M. D., Baudry, A., Richards, A. M. S., et al. 2016, *MNRAS*, **456**, 374
- Greene, J. E., Peng, C. Y., Kim, M., et al. 2010, *ApJ*, **721**, 26
- Greene, J. E., Seth, A., Kim, M., et al. 2016, *ApJL*, **826**, L32
- Greene, J. E., Zakamska, N. L., & Smith, P. S. 2012, *ApJ*, **746**, 86
- Greenhill, L. J. 2004, *NewAR*, **48**, 1079
- Greenhill, L. J., Henkel, C., Becker, R., Wilson, T. L., & Wouterloot, J. G. A. 1995, *A&A*, **304**, 21
- Greenhill, L. J., Kondratko, P. T., Lovell, J. E. J., et al. 2003, *ApJ*, **582**, 11
- Greenhill, L. J., Kondratko, P. T., Moran, J. M., & Tilak, A. 2009, *ApJ*, **707**, 787
- Greenhill, L. J., Tilak, A., & Madejski, G. 2008, *ApJ*, **686**, 13
- Gültekin, K., Richstone, D. O., & Gebhardt, K. 2009, *ApJ*, **698**, 198
- Hagiwara, Y., Diamond, P. J., & Miyoshi, M. 2002, *A&A*, **383**, 65
- Hagiwara, Y., Diamond, P. J., & Miyoshi, M. 2003, *A&A*, **400**, 457
- Haschick, A. D., Baan, W. A., & Peng, E. W. 1994, *ApJ*, **437**, 35
- Henkel, C., Guesten, R., Downes, D., et al. 1984, *A&A*, **141**, 1
- Henkel, C., Wouterloot, J. G. A., & Bally, J. 1986, *A&A*, **155**, 193
- Herrnstein, J. R., Moran, J. M., Greenhill, L. J., et al. 1999, *Natur*, **400**, 539
- Herrnstein, J. R., Moran, J. M., Greenhill, L. J., & Trotter, A. S. 2005, *ApJ*, **629**, 719
- Hu, W. 2005, in ASP Conf. Ser. 339, Observing Dark Energy, ed. S. C. Wolff & T. R. Lauer (San Francisco, CA: ASP), **215**
- Humphreys, E. M. L., Reid, M. J., Greenhill, L. J., Moran, J. M., & Argon, A. L. 2008, *ApJ*, **672**, 800
- Humphreys, E. M. L., Reid, M. J., Moran, J. M., Greenhill, L. J., & Argon, A. L. 2013, *ApJ*, **775**, 13
- Hutchings, J. B., Crenshaw, D. M., Kaiser, M. E., et al. 1998, *ApJ*, **492**, 115
- Impellizzeri, C. M. V., McKean, J. P., Castangia, P., et al. 2008, *Natur*, **456**, 927
- Jarrett, T. H., Cohen, M., & Masci, F. 2011, *ApJ*, **735**, 112
- Kang, D., Woo, J.-H., & Bae, H. 2017, *ApJ*, **845**, 131
- Kauffmann, G., Heckman, T. M., & Tremonti, C. 2003, *MNRAS*, **346**, 1055
- Kewley, L. J., Groves, B., Kauffmann, G., & Heckman, T. 2006, *MNRAS*, **372**, 961
- Kondratko, P. T., Greenhill, L. J., & Moran, J. M. 2006, *ApJ*, **638**, 100
- Kuo, C. Y., Braatz, J. A., Condon, J. J., et al. 2011, *ApJ*, **727**, 20
- Kuo, C. Y., Braatz, J. A., Lo, K. Y., et al. 2015, *ApJ*, **800**, 26
- Kuo, C. Y., Braatz, J. A., Reid, M. J., et al. 2013, *ApJ*, **767**, 155
- Lacy, M., Storrie-Lombardi, L. J., & Sajina, A. 2004, *ApJS*, **154**, 166
- Liu, X., Zakamska, N. L., Greene, J. E., et al. 2009, *ApJ*, **702**, 1098
- Liu, Z. W., Zhang, J. S., Henkel, C., et al. 2017, *MNRAS*, **466**, 1608
- Lo, K. Y. 2005, *ARA&A*, **43**, 625
- Lupton, R., Gunn, J. E., Ivezić, Z., Knapp, G. R., & Kent, S. 2001, ASPC, **238**, 269
- Marconi, A., & Hunt, L. K. 2003, *ApJ*, **589**, 21
- Masini, A., Comastri, A., & Baloković, M. 2016, *A&A*, **589**, 59
- Mateos, S., Alonso-Herrero, A., Carrera, F. J., et al. 2012, *MNRAS*, **426**, 3271
- Miyoshi, M., Moran, J., Herrnstein, J., et al. 1995, *Natur*, **373**, 127
- Nakai, N., Sato, N., & Yamauchi, A. 2002, *PASJ*, **54**, 27
- Namekata, D., & Umemura, M. 2016, *MNRAS*, **460**, 980
- Neufeld, D. 2000, *ApJ*, **542**, 99
- Neufeld, D. A., & Maloney, P. R. 1995, *ApJ*, **447**, 17
- Neufeld, D. A., Maloney, P. R., & Sara, C. 1994, *ApJ*, **436**, 127
- Olling, R. P. 2007, *MNRAS*, **378**, 1385
- Ott, J., Meier, D. S., & McCoy, M. 2013, *ApJ*, **771**, 41
- Peck, A. B., Henkel, C., Ulvestad, J. S., et al. 2003, *ApJ*, **590**, 149
- Pesce, D. W., Braatz, J. A., Condon, J. J., et al. 2015, *ApJ*, **810**, 65
- Pier, J. R., Munn, J. A., Hindsley, R. B., et al. 2003, *AJ*, **125**, 1559
- Reid, M. J., Braatz, J. A., Condon, J. J., et al. 2013, *ApJ*, **767**, 154
- Riess, A. G., Macri, L. M., Hoffmann, S. L., et al. 2016, *ApJ*, **826**, 56
- Rovilos, E., Fotopoulou, S., Salvato, M., et al. 2011, *A&A*, **529**, 135
- Ruiz, J. R., Crenshaw, D. M., Kraemer, S. B., et al. 2001, *AJ*, **122**, 2961
- Rupke, D. S., Veilleux, S., & Sanders, D. B. 2005, *ApJ*, **632**, 751
- Satyapal, S., Ellison, S. L., McAlpine, W., et al. 2014, *MNRAS*, **441**, 1297
- Schawinski, K., Thomas, D., Sarzi, M., et al. 2007, *MNRAS*, **382**, 1415
- Schawinski, K., Urry, C. M., & Virani, S. 2010, *ApJ*, **711**, 284
- Schlegel, D. J., Finkbeiner, D. P., & Davis, M. 1998, *ApJ*, **500**, 525
- Shakura, N. I., & Sunyaev, R. A. 1973, *A&A*, **24**, 337
- Shimasaku, K., Fukugita, M., & Doi, M. 2001, *AJ*, **122**, 1238
- Spergel, D. N., Bean, R., & Doré, O. 2007, *ApJS*, **170**, 377
- Stern, D., Assef, R. J., & Benford, D. J. 2012, *ApJ*, **753**, 30
- Stern, D., Eisenhardt, P., & Gorjian, V. 2005, *ApJ*, **631**, 163
- Stoughton, C., Lupton, R. H., & Bernardi, M. 2002, *AJ*, **123**, 485
- Strateva, I., Ivezić, Z., Knapp, G. R., et al. 2001, *AJ*, **122**, 1861
- Tremaine, S. 2002, *ApJ*, **574**, 740
- Ulrich, M.-H., Maraschi, L., & Urry, C. M. 1997, *ARA&A*, **35**, 445

- van den Bosch, R. C. E., & de Zeeuw, P. T. 2010, [MNRAS](#), **401**, 1770
- van den Bosch, R. C. E., Greene, J. E., Braatz, J. A., Constantin, A., & Kuo, C.-Y. 2016, [ApJ](#), **819**, 11
- Veilleux, S., & Osterbrock, D. E. 1987, [ApJS](#), **63**, 295
- Whiteoak, J. B., & Gardner, F. F. 1986, [MNRAS](#), **222**, 513
- Woo, J.-H., Bae, H.-J., Son, D., & Karouzos, M. 2016, [ApJ](#), **817**, 108
- Wright, E. L., Eisenhardt, P. R. M., & Mainzer, A. K. 2010, [AJ](#), **140**, 1868
- York, D. G., Adelman, J., & Anderson, J. E. 2000, [AJ](#), **120**, 1579
- Zhang, J. S., Henkel, C., Guo, Q., & Wang, J. 2012, [A&A](#), **538**, 152
- Zhang, J. S., Henkel, C., Guo, Q., Wang, H. G., & Fan, J. H. 2010, [ApJ](#), **708**, 1528
- Zhang, J. S., Henkel, C., Kadler, M., et al. 2006, [A&A](#), **450**, 933
- Zhu, G., Zaw, I., Blanton, M. R., & Greenhill, L. J. 2011, [ApJ](#), **742**, 73